Critical review of partial volume correction methods in PET and SPECT imaging : benefits, pitfalls, challenges, and future outlook

Azimi, Mohammad Saber; Rahmim, Arman; Arabi, Hossein; Sanaat, Amirhossein; Zeraatkar, Navid; Bouchareb, Yassine; Liu, Chi; Alavi, Abass; King, Michael; Boellaard, Ronald; Zaidi, Habib

How to cite

AZIMI, Mohammad Saber et al. Critical review of partial volume correction methods in PET and SPECT imaging : benefits, pitfalls, challenges, and future outlook. In: European journal of nuclear medicine and molecular imaging, 2025, vol. 53, n° 4, p. 2830–2861. doi: 10.1007/s00259-025-07612-5

This publication URL: https://archive-ouverte.unige.ch/unige:189676

Publication DOI: 10.1007/s00259-025-07612-5

European Journal of Nuclear Medicine and Molecular Imaging
https://doi.org/10.1007/s00259-025-07612-5

REVIEW ARTICLE

Critical review of partial volume correction methods in PET and SPECT imaging: benefits, pitfalls, challenges, and future outlook

Mohammad Saber Azimi[1] · Arman Rahmim[2] · Hossein Arabi[3] · Amirhossein Sanaat[3] · Navid Zeraatkar[4] · Yassine Bouchareb[5] · Chi Liu[6] · Abass Alavi[7] · Michael King[4] · Ronald Boellaard[8] · Habib Zaidi[3,9,10,11,12]

Received: 5 June 2025 / Accepted: 25 September 2025

Abstract

Purpose Partial volume effects (PVE) remain a major challenge in quantitative single-photon emission computed tomography (SPECT) and positron emission tomography (PET) imaging, often compromising both accuracy and reproducibility. While numerous Partial Volume Correction (PVC) methods have been proposed, their clinical translation is still limited. This review provides a clinically oriented evaluation of PVC methods with a particular focus on state-of-the-art applications in neurology, cardiovascular imaging, oncology, and radiopharmaceutical therapy dosimetry, highlighting where these techniques offer the greatest added value. In addition, we outline which PVC techniques have the potential to be used in clinical practice and which remain primarily suited for research purposes, along with their suitability in each of the above-mentioned clinical domains. Finally, this review addresses the central question of whether PVC is essential in clinical practice or whether its impact is context dependent.

Methods This review categorizes PVC approaches into three partially overlapping classes: reconstruction-based, post-reconstruction-based, and AI-driven or hybrid methods. Each class is further divided into anatomical and non-anatomical subcategories. We systematically compare their clinical applicability across key dimensions: quantitative accuracy, lesion detectability, robustness to noise and artifacts, anatomical dependence, generalizability across scanners and tracers, and clinical readiness.

Results PVC techniques often improve quantitative accuracy in small structures and in regions affected by spill-over from adjacent high-uptake tissues. However, these benefits can come at the cost of increased noise or edge artifacts, which may limit their robustness for routine clinical use. Post-reconstruction methods are sensitive to segmentation errors, while AI-driven models, despite their promise, require further validation using clinical benchmarks, comparison to ground truth, and testing on diverse datasets. Issues, such as generalizability and interpretability remain significant barriers.

✉ Habib Zaidi
habib.zaidi@hcuge.ch

[1] Department of Medical Radiation Engineering, Shahid Beheshti University, Tehran, Iran

[2] Departments of Radiology and Physics, University of British Columbia, Vancouver, BC, Canada

[3] Division of Nuclear Medicine & Molecular Imaging, Geneva University Hospital, Geneva CH-1211, Switzerland

[4] Department of Radiology, University of Massachusetts Chan Medical School, Worcester, MA, USA

[5] Department of Radiology & Molecular Imaging, College of Medicine and Health Sciences, Sultan Qaboos University, Muscat 123, Oman

[6] Department of Radiology and Biomedical Imaging, Yale University, New Haven, CT, USA

[7] Department of Radiology, Perelman School of Medicine, University of Pennsylvania, Philadelphia, PA, USA

[8] Department of Radiology and Nuclear Medicine, Amsterdam UMC location Vrije Universiteit Amsterdam, Amsterdam, The Netherlands

[9] Department of Nuclear Medicine and Molecular Imaging, University of Groningen, University Medical Center Groningen, Groningen, Netherlands

[10] Department of Nuclear Medicine, University of Southern Denmark, Odense, Denmark

[11] University Research and Innovation Center, Óbuda University, Budapest, Hungary

[12] Division of Nuclear Medicine and Molecular Imaging, Geneva University Hospital, Geneva CH-1211, Switzerland

Published online: 05 November 2025

Conclusion This review emphasizes the importance of application-tailored PVC protocols for reliable quantitative imaging in neurology, cardiology, oncology, and radiopharmaceutical therapy dosimetry. Not all PVC methods are beneficial; some may even impair interpretation in certain contexts. We provide a practical overview of which PVC approaches are most beneficial for each clinical scenario, aiming to guide both researchers and clinicians in selecting appropriate techniques for future studies and routine practice, and also outline key areas requiring further development for broader integration into research and clinical workflows.

Graphical abstract

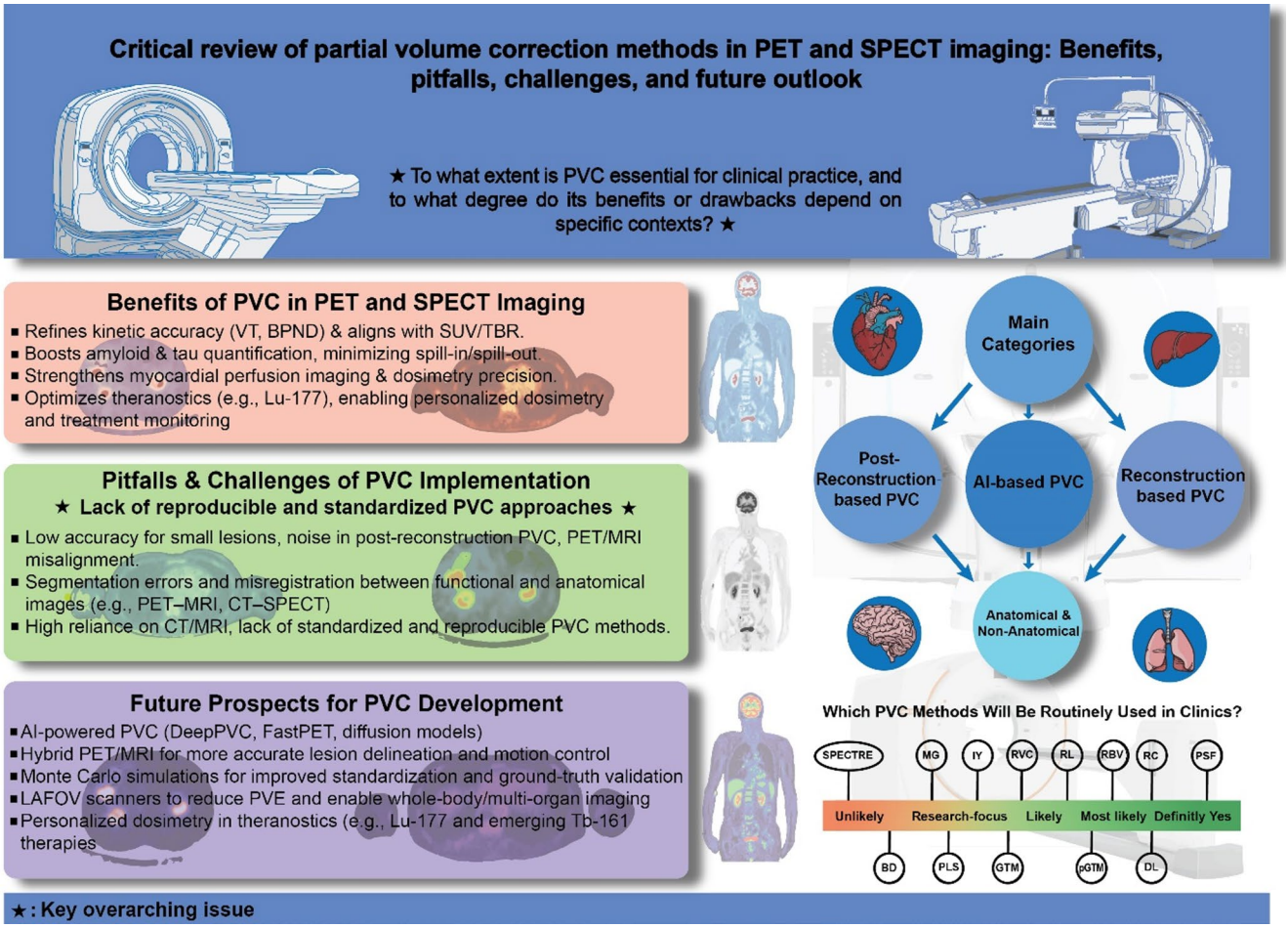

Keywords PET · SPECT · Partial volume correction (PVC) · Image reconstruction · Anatomical information · Quantitative imaging

Introduction

Positron emission tomography (PET) and single-photon emission computed tomography (SPECT) play crucial roles in functional imaging for a wide variety of clinical indications including neurology, cardiology, and oncology by visualizing metabolic and molecular processes in vivo [1–4]. However, their quantitative accuracy is limited by the partial volume effect (PVE), which stems from the finite spatial resolution of imaging systems. As shown in Fig. 1A, PVE leads to signal spill-over and underestimation of tracer uptake in small or adjacent structures, especially when their size is equal to or smaller than 2–3 times the full-width-at-half-maximum (FWHM) of the imaging system [1, 2, 5–7]. In typical clinical setting, the FWHM values range from 3 to 6 mm for PET scanners and from 7 to 12 mm for SPECT systems, depending on the specific system and reconstruction protocols. Therefore, structures smaller than approximately 6–15 mm in PET or 14–25 mm in SPECT are most susceptible to severe PVEs. Even structures marginally larger than FWHM can suffer partial volume losses due to spill-over effects and motion-related artifacts from

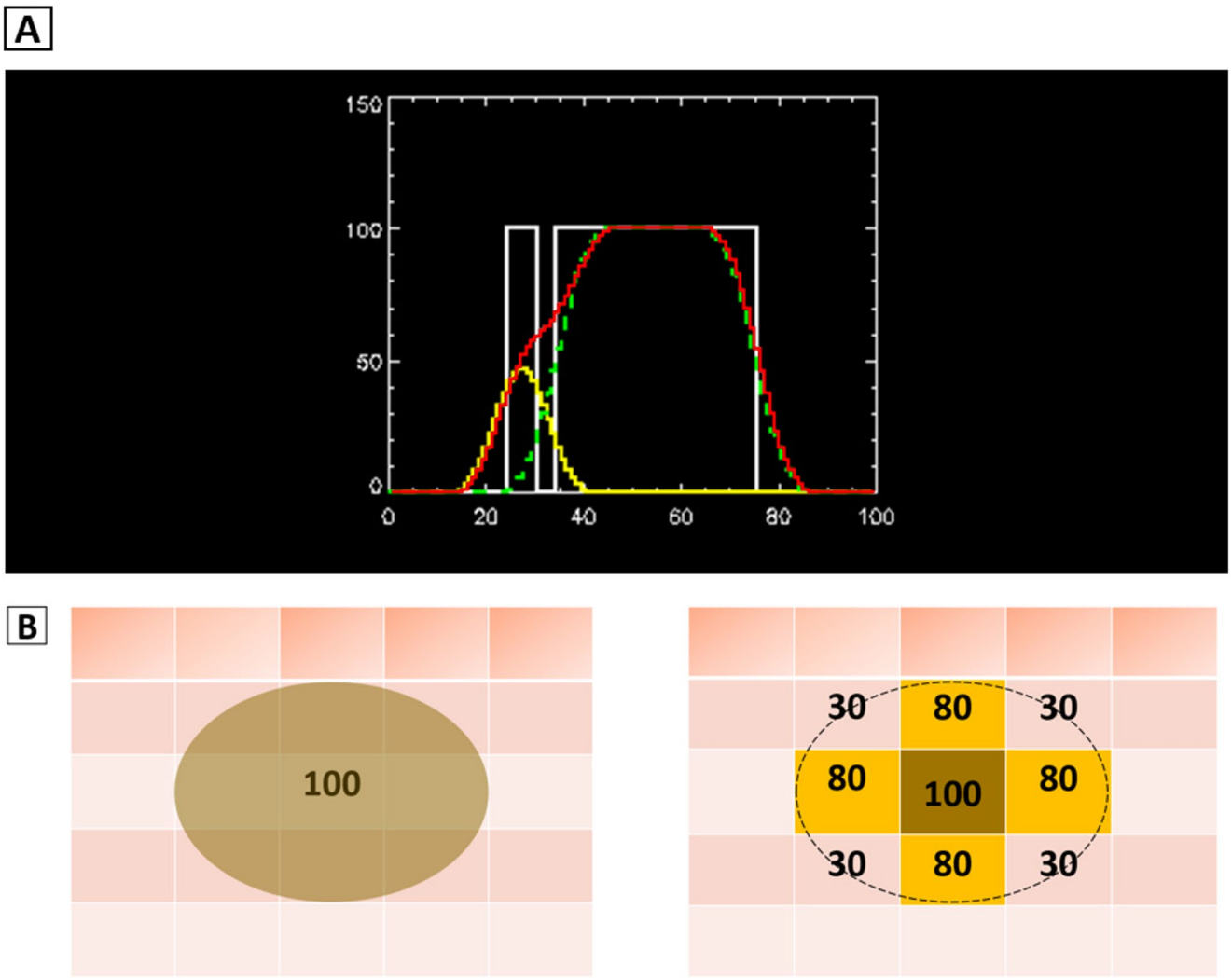

Fig. 1 Depiction of the partial volume effect (PVE) in medical imaging. (**A**) A one-dimensional illustration of the PVE. The x-axis represents the position along a line profile through adjacent structures, and the y-axis represents the relative activity concentration. The white lines represent the relative concentration of activity in two structures with the same activity concentration but of different widths, separated by a narrow non-activity region. The yellow line represents a thin structure whose width is 2–3 times smaller than the full-width-at-half-maximum (FWHM) of the system, blurred by the spatial resolution of PET or SPECT imaging. Its maximum value is reduced to about half the true value, with activity spilling into adjacent regions (spill-out) and partly into the neighbouring thicker structure (spill-in). The green line represents a larger structure, where the centre activity is preserved but edges are underestimated due to spill-out. The red line shows the total activity profile (sum of thin and thick structures), illustrating how adjacent structures are blurred together. (**B**) Illustration of the tissue-fraction effect: tracer distribution sampled on a voxel grid where voxel boundaries do not align with the actual structure, leading to partial volume averaging

cardiac or respiratory activity, underlining the relevance of motion correction algorithms [8–18]. Figure 1B illustrates the impact of voxel size and the resulting tissue-fraction effect at structure boundaries. While both PET and SPECT are affected by PVEs, PET generally offers higher spatial resolution and sensitivity, whereas SPECT is more prone to scatter and collimator-related distortions [19]. As a result, Partial Volume Correction (PVC) strategies optimised for one modality may not directly translate to the other [20]. In SPECT, lower resolution makes PVE more pronounced, particularly in cardiac imaging, dosimetry, and small-lesion quantification [21–23], and advanced techniques such as blood-concentration-based or iterative multi-target correction (MTC) can improve accuracy but remain computationally intensive [24–26].

Addressing PVE improves PET/SPECT accuracy. This can be achieved by enhancing scanner resolution or modelling resolution effects during reconstruction [27–31]. PVC techniques, ranging from region-based (RB) to advanced iterative and reconstruction-integrated methods, provide more elaborate correction [32–45]. Recent studies emphasize the value of post-processing and AI-enhanced

reconstruction methods for PVC. Deep learning (DL) techniques show promise in low-dose and high-resolution imaging, and PVC is increasingly recognized as vital in oncology, brain segmentation, radionuclide therapy, and radiation treatment planning, by improving absorbed dose calculation accuracy and lesion delineation [46–51].

Instead of simply updating the comprehensive review published in Physics in Medicine and Biology 13 years ago [34], this review provides a broad and up-to-date survey of PVC in PET and SPECT imaging across neurology, cardiology, and oncology. Our aim is to highlight strengths, limitations, and real-world applicability of PVC methods, with a particular focus on their role in clinical workflows, an aspect not systematically addressed in previous reviews. PVC techniques are categorized into three main groups, reconstruction-based, post-reconstruction-based, and hybrid/AI-based approaches, each with guided or unguided variants. While prior studies have described these methods, significant gaps remain in systematically comparing them across clinical domains and clarifying their deployment in practice. This review addresses these gaps and explores the critical question: Is PVC essential and indispensable for clinical practice, or does its impact vary depending on context, with the potential to be either beneficial or detrimental?

To enable structured comparison, we introduce a ten-category classification framework based on three core dimensions: imaging modality (PET or SPECT), anatomical guidance (guided vs. unguided), and algorithmic approach (conventional vs. AI/hybrid). While a direct combination of these binary dimensions would yield eight categories, the inclusion of hybrid methods, particularly those integrating AI into both reconstruction and post-reconstruction stages, results in ten practically distinct groupings. This framework allows systematic grouping and nuanced comparison of PVC methods across contexts, acknowledging methodological overlaps and highlighting where certain techniques excel. Following the review of existing studies, the discussion section (section V) provides an overall assessment of different PVC techniques, exploring their advantages, limitations, challenges, and opportunities for future application in diverse clinical settings (the reader can immediately skip to that section for a bird's-eye view of status and prospects of PVC. In particular, we provide Tables in section V summarizing most common PVC algorithms categorized by their benefits, pitfalls, and likelihood of routine clinical deployment). Finally, the conclusion summarizes insights into the overall role of PVC in PET and SPECT imaging, providing a nuanced perspective on its relevance and implications for clinical adoption.

Overview of partial volume correction strategies

Over the years, PVC methodologies have advanced significantly, leveraging high-resolution anatomical information from CT or MRI to mitigate PVE and improve quantitative PET and SPECT accuracy. These approaches fall into two main categories: post-reconstruction and reconstruction-integrated techniques.

Post-reconstruction strategies include regional methods (e.g., Recovery Coefficient (RC) [1], Geometric Transfer Matrix (GTM) [12]) that correct predefined homogeneous regions, and voxel-wise approaches (e.g., Müller-Gärtner (MG) [52], Region-Based Voxel-Wise (RBV) [33], image deconvolution [53]) aimed at restoring localized activity and reducing spill-over. Sinogram-domain methods correct directly on projection data before reconstruction, benefiting from reduced spatial noise correlation and more tractable pipelines [54–57]. Reconstruction-based methods incorporate the system's point spread function (PSF) into image formation, inherently adjusting for PVE and improving structural fidelity [58]. At the cutting edge, AI-based and simulation-supported strategies are reshaping PVC innovation [59–61]. DL models can adaptively restore resolution from large datasets, while phantom-based simulations provide controlled environments for development and benchmarking [62]. These methodologies are summarized in Fig. 2 summarizes the distribution of the 192 reviewed studies according to imaging modality (PET vs. SPECT), PVC implementation stage (reconstruction, post-reconstruction, or hybrid/AI), and anatomical guidance (anatomical vs. non-anatomical). This visual mapping highlights methodological diversity across the literature, as well as dominant trends in clinical applications and algorithmic strategies.

PVC approaches in PET imaging

Reconstruction-based PVC in PET imaging

Reconstruction-based PVC techniques integrate PVE correction directly into the image reconstruction process, thereby improving resolution, quantitative accuracy, and noise characteristics. Depending on the use of anatomical priors (e.g., MRI, CT), they can be categorized into anatomically-guided and non-anatomically-guided approaches. PET-specific applications: In PET, these methods are particularly advantageous in neurology, cardiology, and oncology, where accurate small-structure quantification is critical [63–101]. A comparative overview of PET reconstruction-based PVC strategies is provided in Supplementary Table S1.

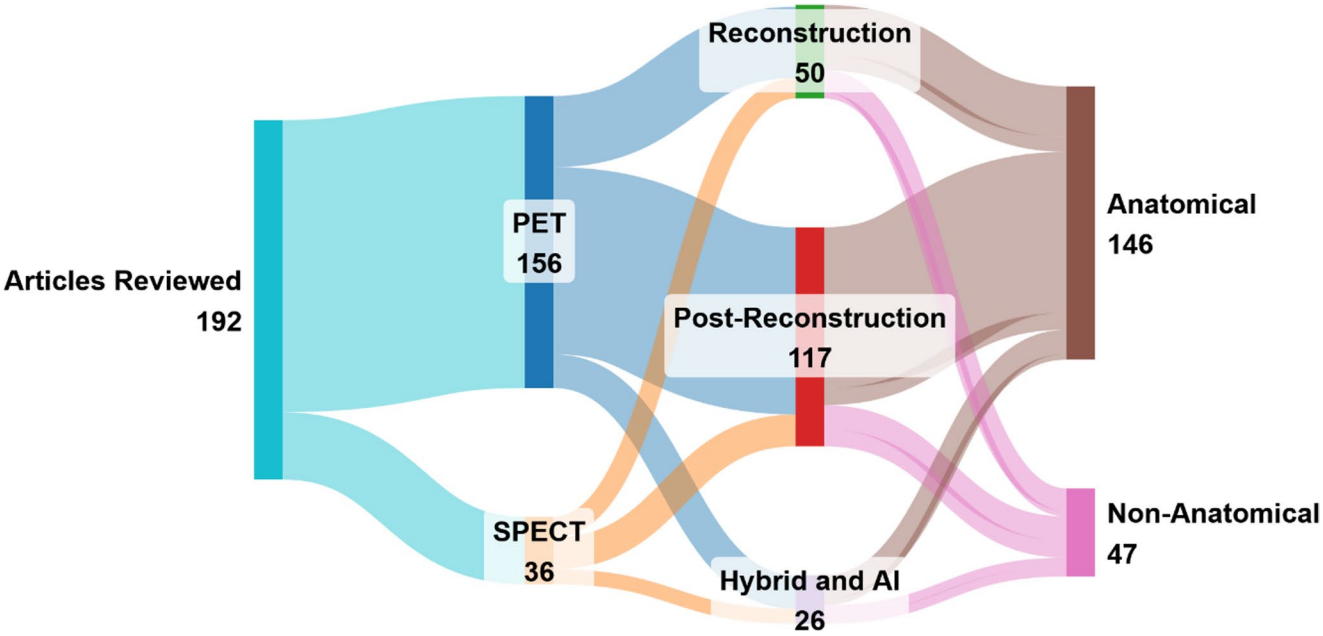

Fig. 2 Sankey diagram illustrating the classification of the 192 reviewed articles by imaging modality (PET, SPECT), PVC implementation stage (reconstruction-based, post-reconstruction, or hybrid/AI-based), and anatomical guidance (anatomical vs. non-anatomical). Flow widths are proportional to the number of studies in each category, revealing that most PET studies employed anatomically guided post-reconstruction PVC, while non-anatomical methods remain less represented

Anatomically guided reconstruction-based PVC

These approaches embed high-resolution anatomical information, most often from MRI, and occasionally CT, into the PET reconstruction process to reduce PVEs. MRI is frequently preferred for its superior soft tissue contrast, enabling more accurate resolution recovery, lesion detectability, and quantification. Studies have consistently shown that anatomical priors improve PET accuracy: for instance, Vunckx et al. [63] reported that the Bowsher prior enhanced spatial resolution by 15–20% and reduced SUV bias in small cortical regions, while Gutierrez et al. [64] achieved PVE errors below 5% in small brain structures using MRI-guided voxel-based PVC. Other works have integrated advanced priors, such as joint entropy [65, 66] or Markov random fields [67], into reconstruction, balancing noise suppression with detail preservation. MRI-guided methods have proven effective across brain, cardiac, and oncological PET, with applications in tau/amyloid quantification, dopamine transporter imaging, and tumour metabolic activity assessment. Despite these benefits, performance depends heavily on high-quality anatomical data, accurate PET/MRI registration, and reliable segmentation; errors in these steps can induce quantification bias. Computational demands are higher than for non-anatomical methods, but in anatomically rich regions, these techniques remain a gold standard for synergistic PET–MRI reconstructions.

Non-anatomically guided reconstruction-based PVC

In the absence of structural imaging, these methods integrate the system's PSF, statistical priors, or sparsity constraints directly into iterative reconstruction. This enables PVE correction for stand-alone PET systems or cases without MRI/CT. High-resolution PET studies have shown that reconstruction-based PVC methods can improve quantitative accuracy, with within- and post-reconstruction strategies demonstrating benefits in brain FDG data [88]. Further, kernel-based PSF correction approaches have been developed, showing improved PVC performance compared with MR-based methods in brain PET [89]. Quantitative oncology studies reported 10–15% SUV accuracy improvements when applying partial-volume correction during PSF-modelled OSEM reconstruction [92], while generalized PSF modelling further optimized quantitation across a wider range of PET applications [93]. In oncological PET, penalized-likelihood reconstructions enhanced stability of quantitation and improved partial-volume correction [94]. Super-resolution–based methods have also been applied for brain PET, achieving improved correction of partial-volume effects [95]. Finally, dynamic PET

studies demonstrated that resolution modelling significantly improved brain kinetic parameter estimation, particularly for FDG modelling [96].

Post-reconstruction PVC in PET imaging

Post-reconstruction PVC methods apply correction after image reconstruction, using either anatomical priors or intrinsic image properties to mitigate PVEs. This is valuable when advanced reconstruction-based correction is unavailable. PET-specific applications: In PET, these methods have been used extensively across neurological, oncological, and cardiac studies [102–200], as summarized in Supplementary Table S2.

Anatomically guided post- reconstruction-based PVC

These methods apply correction after PET image reconstruction using anatomical priors, often derived from CT or MRI, to improve the accuracy of quantification. They are widely used in oncology, neurology, and cardiology to enhance lesion detectability and biomarker precision. Applications include tau and amyloid imaging in Alzheimer's disease, dopaminergic PET in Parkinson's disease, and brain metabolism mapping. Toolboxes like PETPVC and pipelines such as APPIAN enable standardized implementation, incorporating alignment, segmentation, and quality control. Representative studies highlight their practical impact: Azimi et al. [200] found that radiomic feature reproducibility in brain PET strongly depends on the PVC method, with RVC and RL showing the best stability (>60% features with COV < 25% and ICC ≥ 0.75), while MTC and PLS were least reliable. Gallivanone et al. reported that applying MRI-guided GTM PVC increased tumour SUV_{mean} accuracy by >10% in lung and breast cancer, thereby improving prediction of disease-free survival [110]. Sari et al. [164]. developed a method using MRA and Single-Target Correction (STC) for carotid artery PET-FDG images, restoring at least 92.4% of true signal intensity. Malpas et al. [156] demonstrated that in longitudinal Alzheimer's PET, PVC revealed uptake increases over 24 months that were not visible in uncorrected scans, underlining the need for both corrected and uncorrected data. However, these gains depend heavily on accurate segmentation and high-quality co-registration, with performance sensitive to MRI resolution and artifacts. Figures 3 and 4 illustrate the complete PVC processing workflow (from MRI-based parcellation to corrected PET output) and compare multiple PVC algorithms (e.g., MG, GTM, RBV, SFSRR, modSFSRR) in Alzheimer's disease (AD) and healthy control (HC) datasets, showing that advanced methods, like modSFSRR, yield the lowest bias, especially in small structures, such as the hippocampus.

Non-anatomically-guided post-reconstruction-based PVC

These methods enhance PET quantification using statistical models, deconvolution techniques, and machine learning without requiring additional anatomical data, making them valuable when MRI or CT is unavailable. They have been applied in cardiac PET, tumour response assessment, and brain imaging, where they improve SUVs and regional uptake consistency. Hofheinz et al. [188] introduced a model-free GTM variant that improved lesion SUV accuracy by 15–25% without anatomical priors. Golla et al. [195] found that iterative deconvolution with HYPR denoising improved grey matter VT estimation by 12% compared to uncorrected PET. Mikasa et al. [194] showed that dual-time-point standardization reduced inter-scan SUV variability in oncological PET by up to 10%. Hatt et al. observed that applying PVC increased AUC for predicting therapy response in oesophageal cancer from 0.67 to 0.74 [189], with notable improvements in tumour heterogeneity quantification [190, 192]. Despite these benefits, non-anatomical methods can amplify noise and lack structural guidance in heterogeneous or low-contrast regions. Hybrid strategies that combine statistical modelling with anatomical estimation are emerging to mitigate these issues. Figure 5 demonstrates how iterative deconvolution with HYPR denoising improves grey matter quantification in [^{11}C]FMZ PET. The images and plots show that applying spatial noise *regularisation* or HYPR filtering reduces variability and yields VT estimates closer to reference values across multiple brain regions.

Hybrid and AI-based PVC approaches in PET imaging

Hybrid and AI-based PVC approaches combine classical correction frameworks with machine learning or DL algorithms. These may operate with or without anatomical priors and can augment or replace steps in both reconstruction-based and post-reconstruction-based pipelines. PET-specific applications: PET implementations have shown improvements in small-structure quantification and robustness in multi-tracer studies [201–217]. Detailed examples are summarized in Supplementary Table S3.

Anatomically-guided hybrid and AI-based PVC

Anatomically-guided hybrid PVC methods enhance PET quantification by combining traditional correction strategies

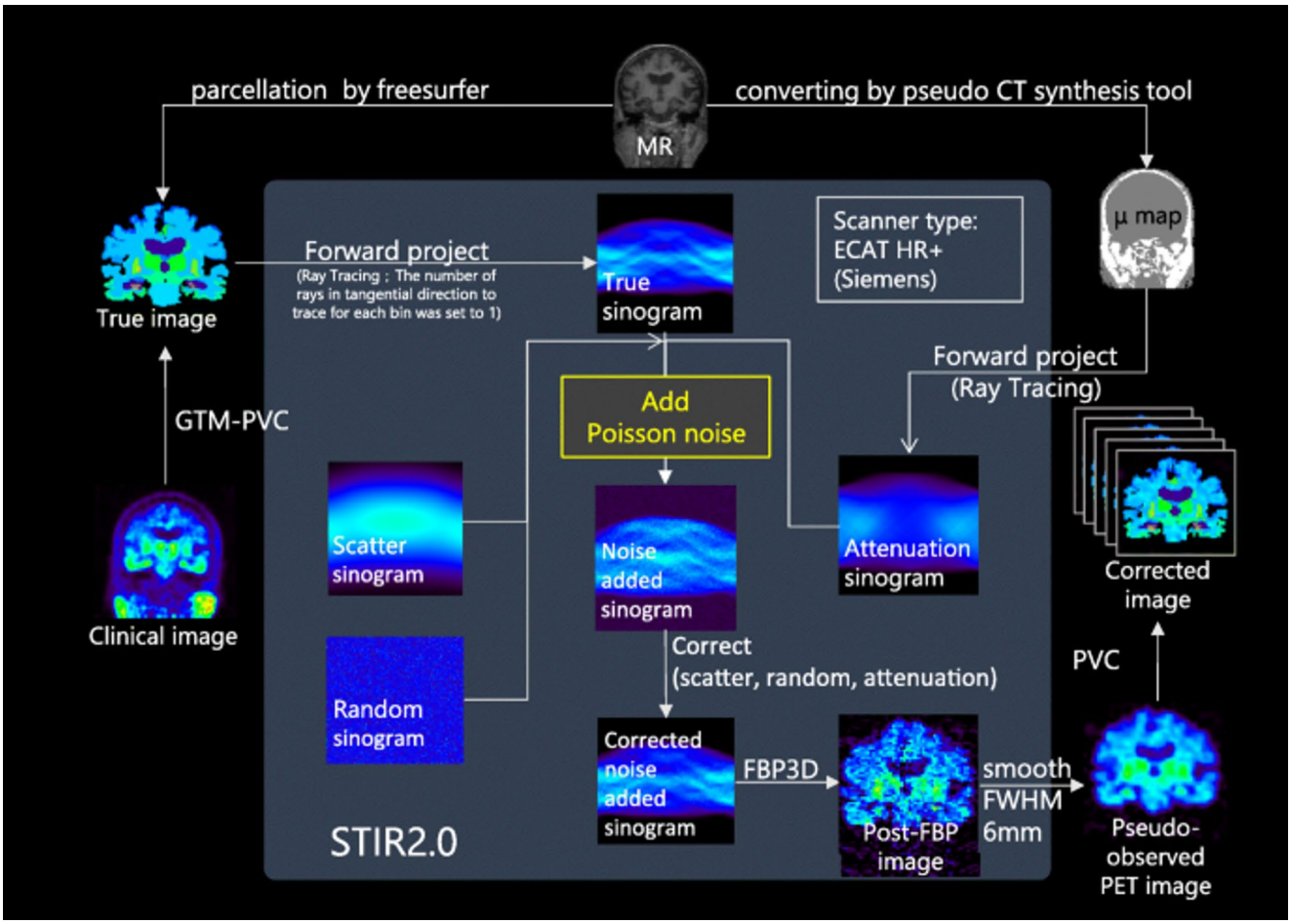

Fig. 3 Workflow of the PET PVC process, starting from MR-based segmentation and μ-map generation, followed by forward projection, noise addition, scatter/attenuation correction, and image reconstruction. PVC is applied in the final step to produce corrected PET images ready for analysis. These schematic highlights how anatomical priors and accurate system modelling are integrated to minimize partial volume effects. Reprinted with permission from [163] under a Creative Commons Attribution License (CC BY 4.0 DEED)

with DL models that exploit structural information from high-resolution modalities, such as MRI. These approaches are especially beneficial in neurological imaging, where precise localization and tissue differentiation are crucial. They have been applied in tracer evaluation, disease phenotyping, and PET/MR synergistic imaging.

Xu et al. [201] developed a multi-step framework combining PET segmentation, denoising, and PVC (using Anscombe transformation, iterative volume-consistent PVC, and clustering), improving clarity and quantification accuracy. Song et al. [202] implemented a super-resolution CNN incorporating MRI-derived priors, achieving improved PET image sharpness compared to conventional methods. Zhao et al. [203] showed that PVC improved ^{18}F-AV1451 tau deposition measurements in small brain regions, thereby enhancing correlation analyses. Corda-D'Incan et al. [211] proposed Syn-Net for synergistic PET-MR reconstruction, achieving both noise reduction and sharper structural boundaries, while Matsubara et al. [205] introduced deepPVC, predicting PVC maps directly from PET and MRI without requiring segmentation, reducing processing time. Lin et al. [217] introduced MRI-styled PET, a deep-learning fusion framework leveraging T1-weighted MRI to enhance FDG-PET structural details and quantitative accuracy degraded by PVE, achieving higher SSIM and PSNR than conventional anatomy-guided PVC and baseline fusion models. Despite improvements in image sharpness, noise reduction, and SUV recovery, these methods remain sensitive to registration quality, anatomical variability, and diversity of training datasets. Figures 6 and 7 show a representative 2D U-Net-based PVC model for brain PET and its application in [^{18}F]-FDG imaging, illustrating architectural components (encoder–decoder, skip connections) and comparative visual results across MR, PET, real PVC, and predicted PVC maps, highlighting consistency in small brain regions and tracer distribution.

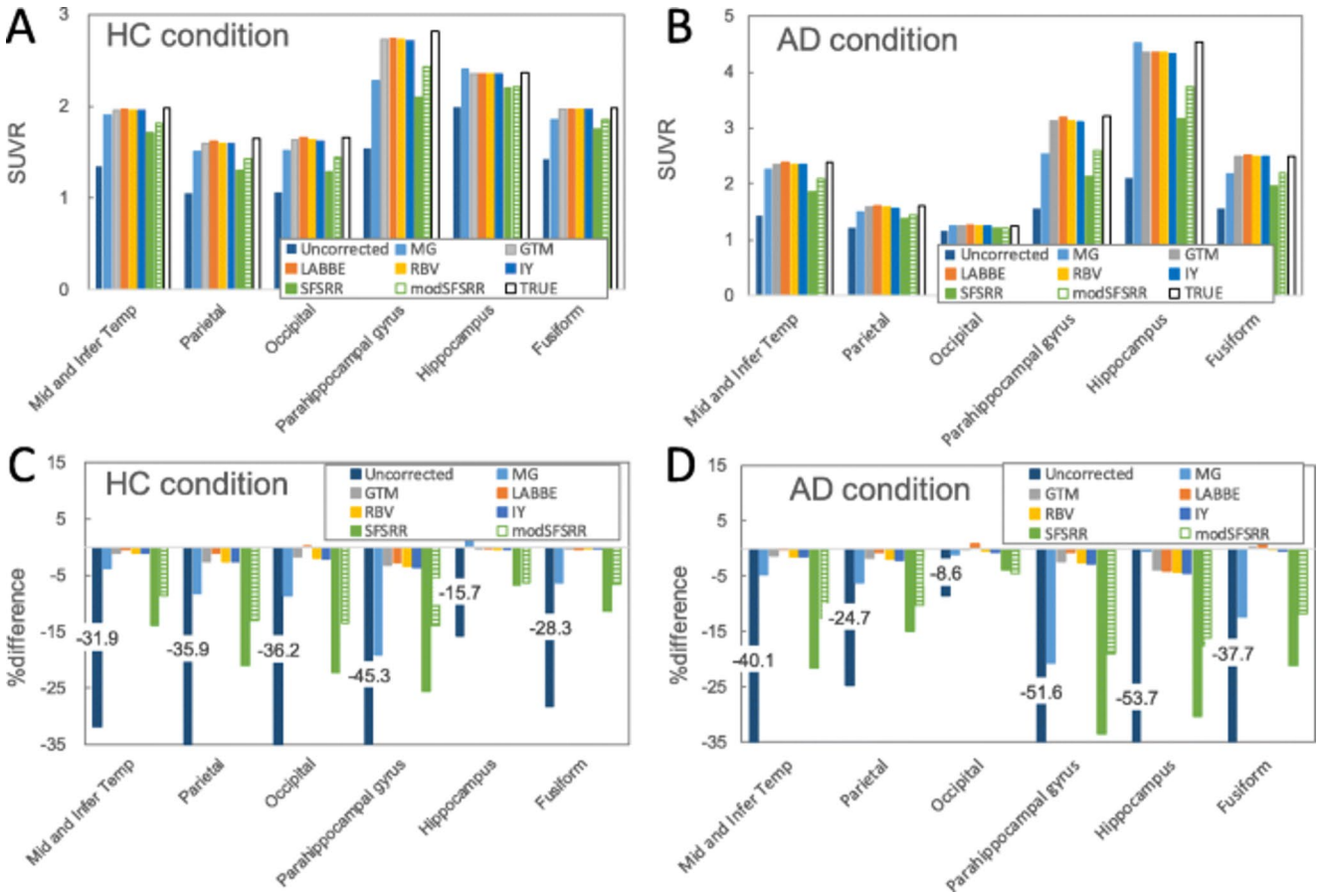

Fig. 4 Comparison of SUVR values and percentage differences between pseudo-observed, PVC-corrected, and true SUVRs in HC (**A, C**) and AD (**B, D**) conditions. Methods tested include MG, GTM, RBV, SFSRR, and modSFSRR. Results show that modSFSRR consistently achieves the smallest deviation from true SUVRs, while uncorrected images have the largest bias, particularly in the hippocampus and parahippocampal gyrus for AD patients. Reprinted with permission from [163] under a Creative Commons Attribution License (CC BY 4.0 DEED)

Non-anatomically-guided hybrid and AI-based PVC

Non-anatomically-guided PVC approaches remove the dependency on structural imaging by leveraging DL, statistical modelling, or generative techniques trained directly on PET data. Marsh et al. [209] demonstrated that incorporating PVC into ^{124}I-CLR1404 PET/CT improved tumour dosimetry and treatment response assessment in head and neck cancer models.

Jomaa et al. [213] combined iterative deconvolution with shearlet transform, improving SNR and recovery coefficients without anatomical priors. Sanaat et al. [214] introduced a CycleGAN-based PVC framework for multi-tracer datasets, transforming non-PVC PET images into PVC-enhanced images rated visually comparable to original PVC outputs (Figs. 8 and 9). Azimi et al. [215, 216] developed DL architectures capable of generating full-dose PVC PET images and attention-based correction for ^{18}F-FDG brain PET, improving image quality without requiring anatomical information.

These models facilitate automated, segmentation-free correction pipelines and show robustness across tracers and acquisition protocols. However, they face challenges in interpretability, generalizability, and standardization of validation pipelines. Performance can vary significantly with scanner characteristics, tracer type, and acquisition conditions, necessitating further multi-centre validation before widespread clinical adoption.

PVC approaches in SPECT imaging

Reconstruction-based PVC in SPECT imaging

Reconstruction-based PVC in SPECT follows the same categorization principles described above. SPECT-specific applications: Particularly important in neurological, cardiac, and skeletal imaging, often incorporating CT-based anatomical priors [218–228]. Key methods are summarized in Supplementary Table S4.

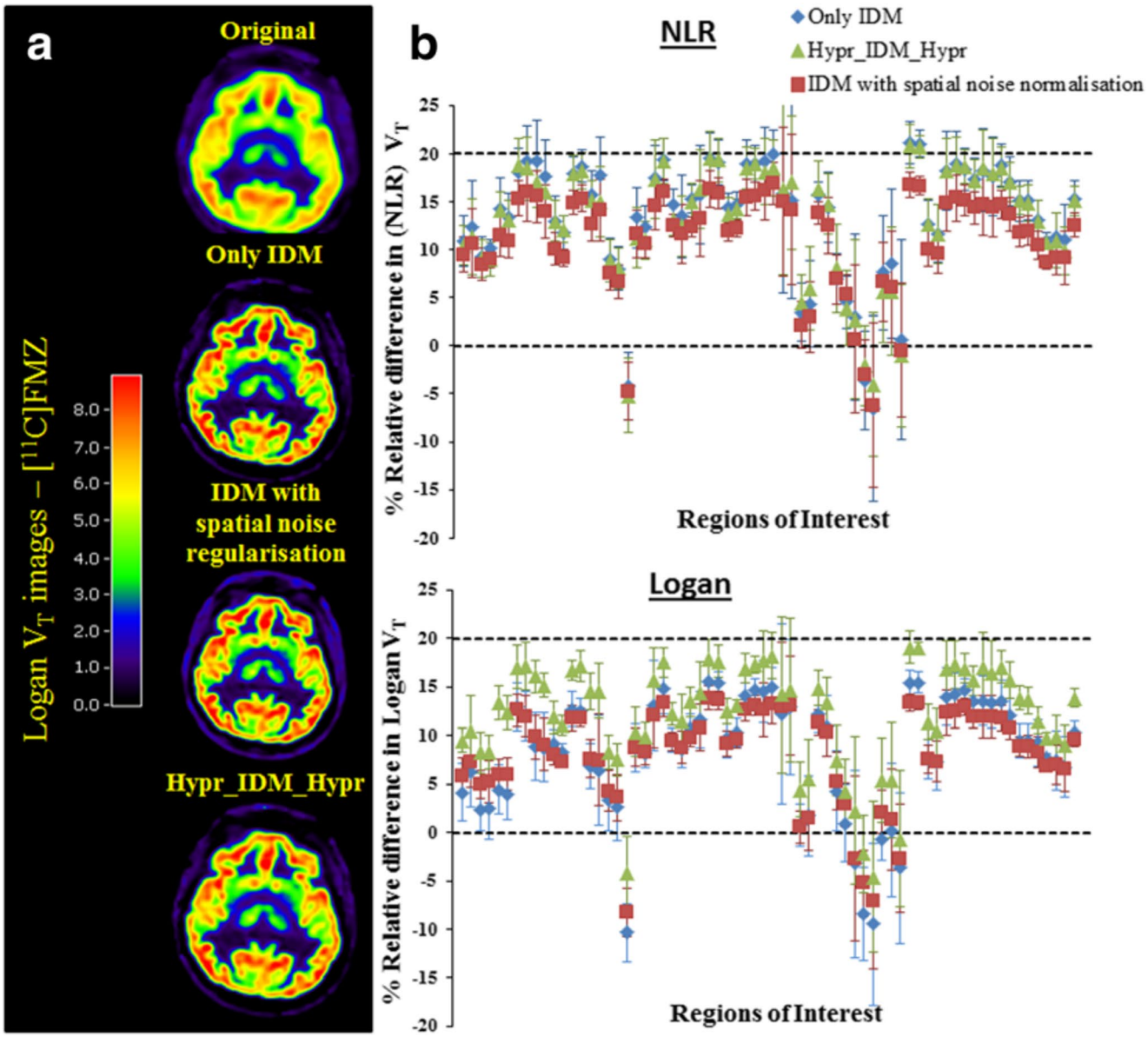

Fig. 5 (**a**) Representative [^{11}C]FMZ VT maps from Logan analysis, comparing uncorrected iterative deconvolution (IDM), IDM with spatial noise regularisation, and IDM with HYPR filtering. (**b**) Regional quantitative effects on VT values computed with both NLR and Logan methods, showing reduced bias and variability after noise suppression, particularly in small cortical structures. This highlights the role of advanced denoising in stabilising post-reconstruction PVC results. Reprinted with permission from [195] under a Creative Commons Attribution License (CC BY 4.0 DEED)

Anatomically-guided reconstruction-based PVC

These methods leverage structural priors (e.g., CT or MRI) to enhance reconstruction accuracy and quantification. They offer strong performance in contrast recovery and lesion detectability, particularly in brain, cardiac, and skeletal imaging. For example, Erlandsson et al. [218] introduced p-PVC for SPECT, correcting for distance-dependent blurring and integrating filtered back-projection (FBP), which improved quantification with faster processing; a follow-up version using OSEM yielded higher striatal contrast (1.53) than both OSEM with resolution recovery (1.42) and standard OSEM (1.04). Chan et al. [220] applied anatomical priors in cardiac SPECT/CT to reduce noise and improve myocardial uptake quantification, while Liu et al. [221] demonstrated enhanced image quality in low-dose cardiac scans with iterative PVC. Kangasmaa et al. [223] showed that Bayesian CT-guided reconstruction methods (AMAP-S and AMAP-R) provided superior accuracy over OSEM for bone SPECT, with lesion-visible CT scans more accurately depicting lesion shape and size. Hybrid approaches such as SPECTRE [224], which uses diagnostic PET to guide

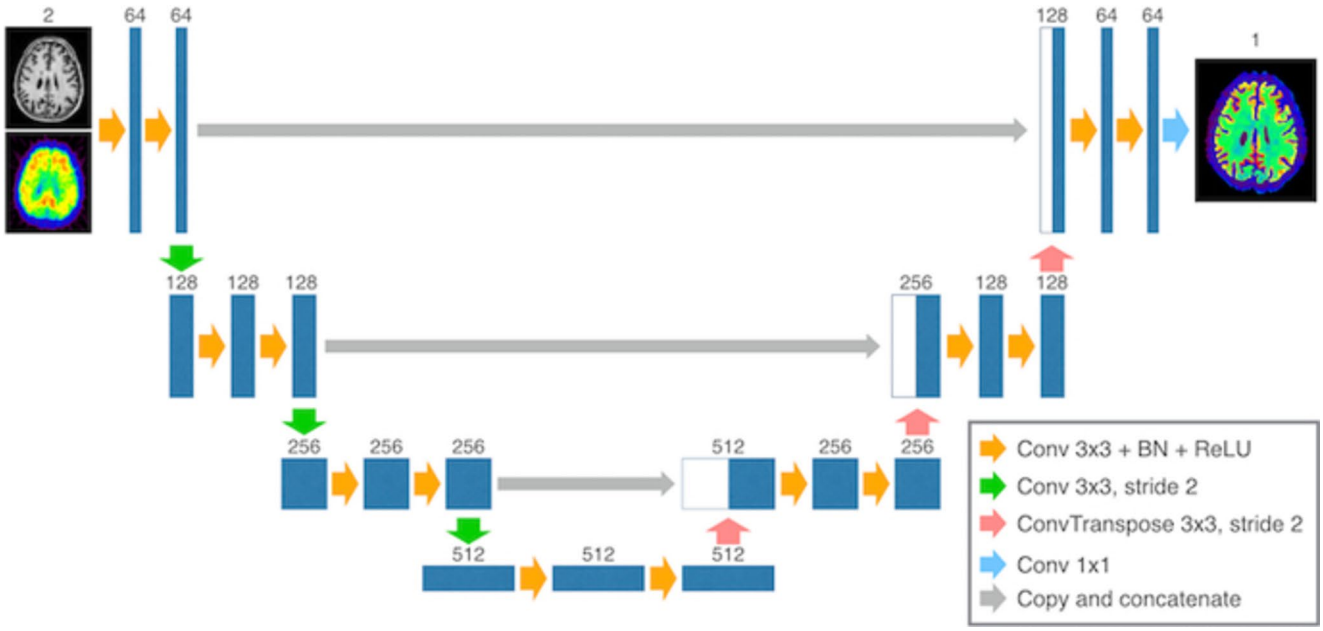

Fig. 6 The 2D U-Net model used for predicting PVC maps in brain PET imaging. It features an encoder-decoder architecture with skip connections, convolutional layers, batch normalization, and ReLU activation. Down-sampling and up-sampling are performed with convolutional layers. This architecture enables accurate PVC prediction while preserving fine structural details. The final output is generated through a 1 × 1 convolutional layer. Numbers indicate the number of channels. Reprinted with permission from [205] under a Creative Commons Attribution License (CC BY 4.0 DEED)

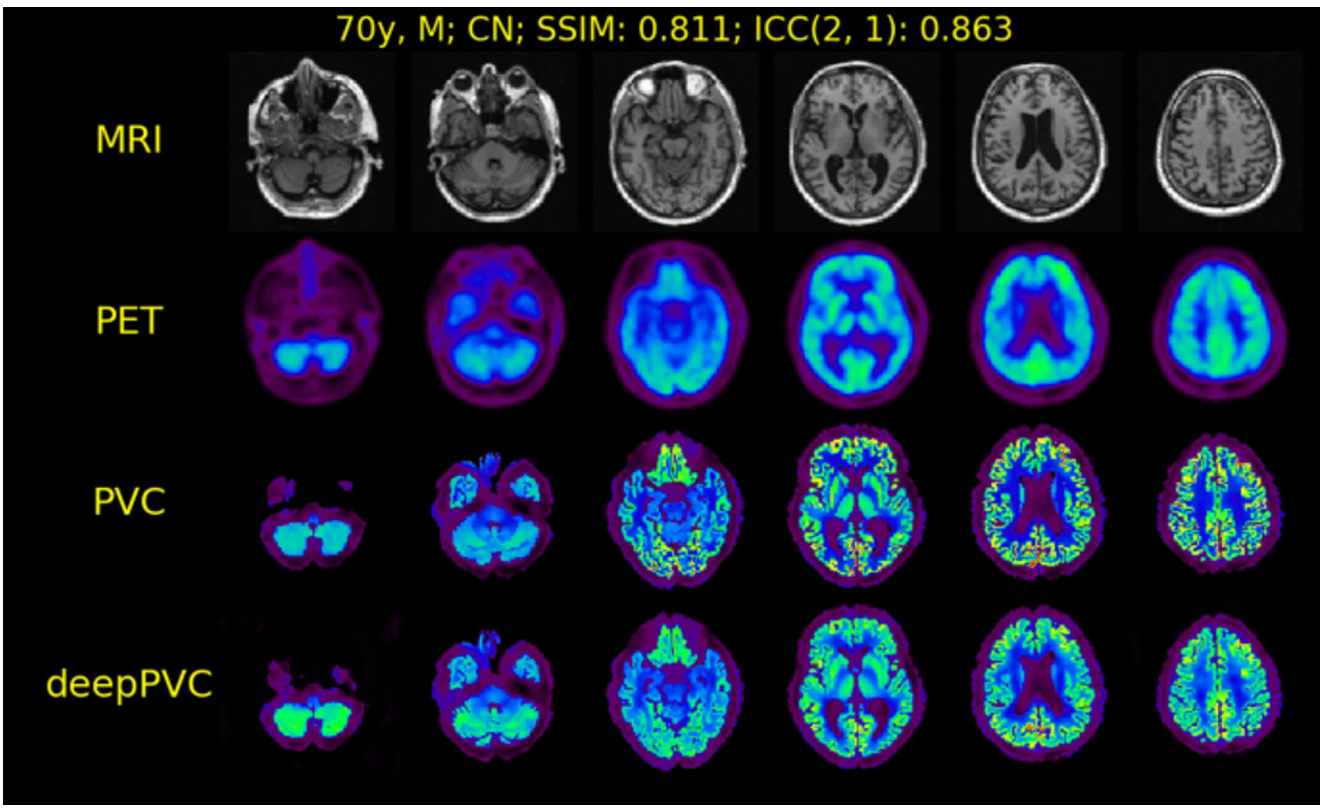

Fig. 7 MR, PET, and both real and predicted PVC maps for instances with the highest ICC in the [^{18}F]-FDG test data. CN stands for cognitively normal; MR for magnetic resonance; PET for positron emission tomography; and PV for partial volume. The deepPVC predictions show high similarity to reference PVC maps, with improved structural definition and contrast in cortical and subcortical regions. Reprinted with permission from [205] under a Creative Commons Attribution License (CC BY 4.0 DEED)

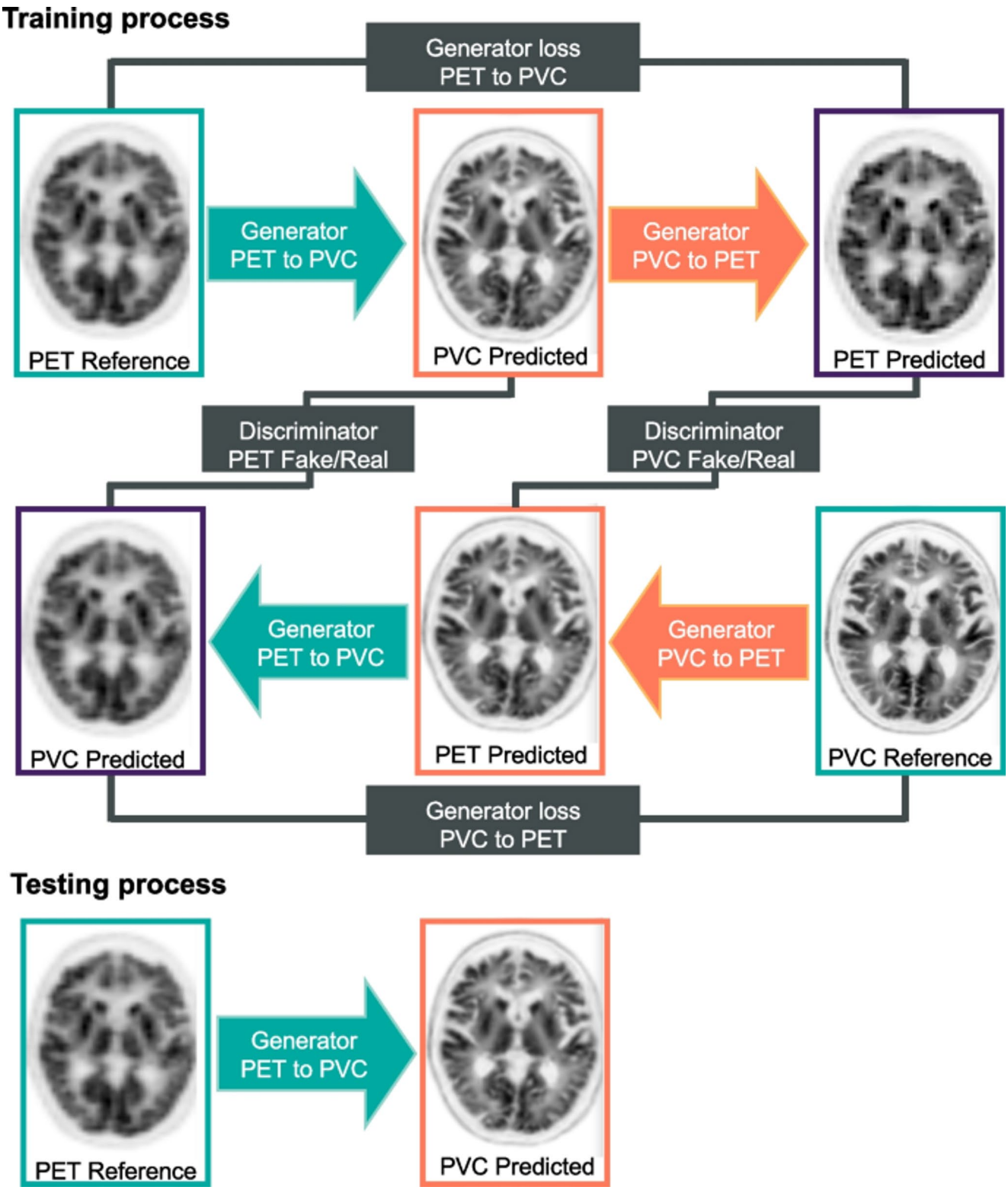

Fig. 8 Schematic representation of the Cycle-GAN architecture for PET-PVC synthesis, illustrating the bidirectional transformation between non-PVC and PVC PET images. The upper panel shows the training procedure, while the lower panel details the testing phase. Reprinted with permission from [214] under a Creative Commons Attribution License (CC BY 4.0 DEED)

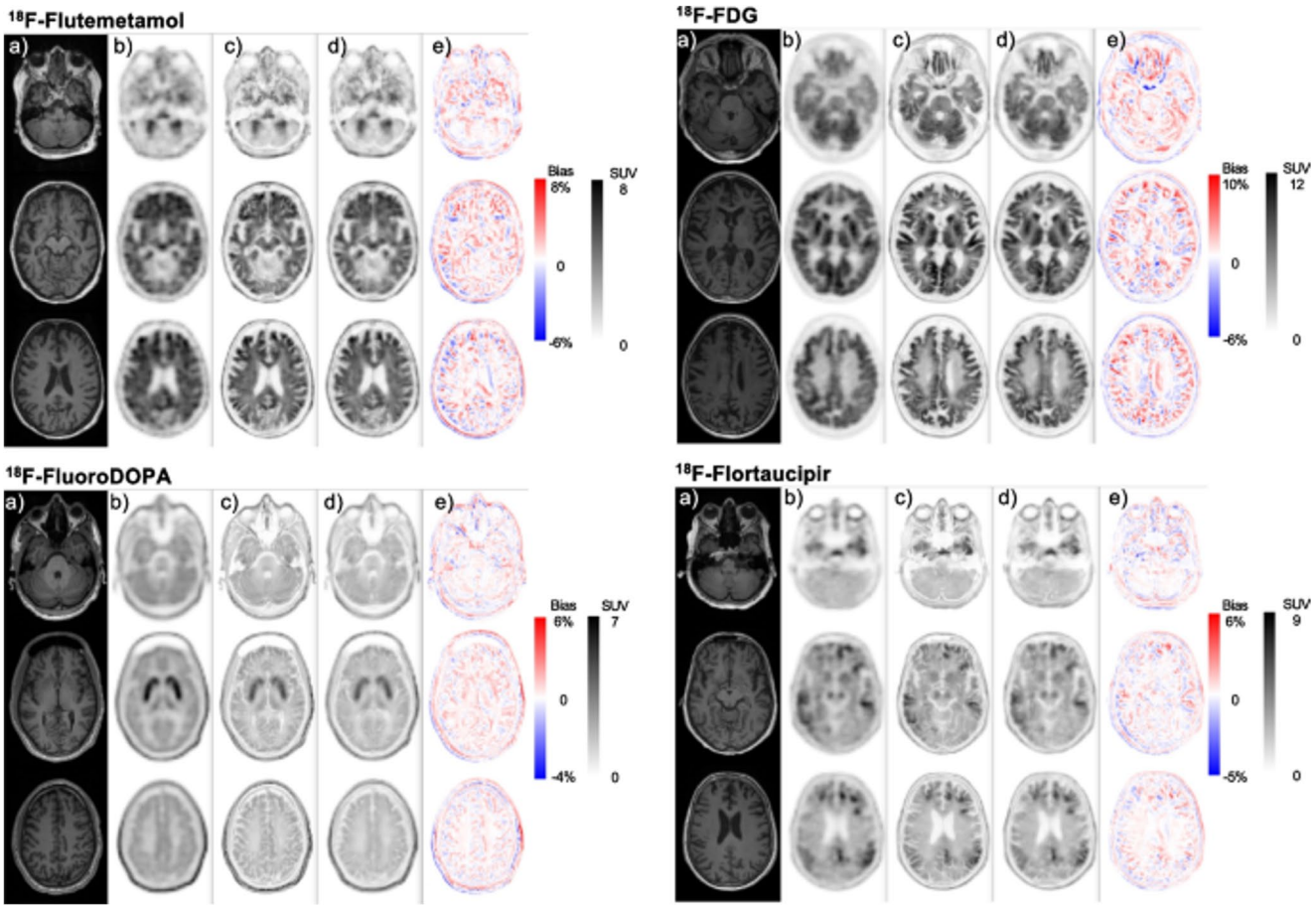

Fig. 9 Example slices from multi-tracer brain PET scans of various patients showcasing: (a) co-registered T1-weighted MRI, (b) non-PVC PET images, (c) MRI-guided reference PVC PET images, (d) DL-predicted PVC PET images, and (e) corresponding bias maps. These results highlight the model's ability to reproduce reference PVC image quality while maintaining tracer-specific uptake patterns. Reprinted with permission from [214] under a Creative Commons Attribution License (CC BY 4.0 DEED)

theranostic SPECT reconstruction, have also improved resolution and dosimetry with reduced noise.

Despite these advantages, anatomically-guided methods remain highly dependent on precise segmentation and registration, making them sensitive to misalignment and anatomical variability, and their computational demands can limit scalability in routine clinical practice.

Non-anatomically-guided reconstruction-based PVC

These techniques rely on physical modelling (e.g., attenuation, scatter, resolution) without requiring anatomical inputs, and are useful when structural imaging is unavailable or unreliable. Morphis et al. [226] used Monte Carlo–based correction for attenuation, scatter, and collimator response in ^{99m}Tc and ^{198}Au SPECT/CT, achieving reliable quantification of small sources. Similarly, Leube et al. [227] reported that resolution modelling in ^{177}Lu-SPECT/CT substantially improved recovery coefficients, especially for small spheres (up to 5.8), though positional variability increased, underlining the need for harmonized acquisition protocols. While such methods are modality-independent and avoid dependency on CT/MRI, they are more susceptible to noise and less effective in recovering small or ambiguous structures. Moreover, despite the accuracy of Monte Carlo simulations, their high computational demands and reduced robustness in complex anatomy still restrict widespread clinical adoption.

Post-reconstruction PVC in SPECT imaging

Post-reconstruction PVC in SPECT is applied in settings where raw projection data are unavailable or reconstruction methods are limited. SPECT-specific applications: Frequently used for brain and myocardial perfusion imaging [21, 22, 24–26, 229–241], with examples listed in Supplementary Table S5. Among post-reconstruction PVC techniques, perturbation-based GTM (pGTM) has shown promise in SPECT for reducing Gibbs artifacts and improving myocardial perfusion imaging. However, challenges

such as CT–SPECT registration errors, resolution mismatches, and difficulty in separating small anatomical structures can still limit accuracy.

Anatomically-guided post-reconstruction-based PVC

These methods apply anatomical priors (typically from CT or MRI) after image reconstruction to correct for PVEs and have shown strong results in cardiac and neurological SPECT. For instance, Liu et al. [229] used an automatic multi-atlas segmentation approach in cardiac SPECT/CT, improving image quality and quantification; Ren et al. [232] optimized PVC factors in ^{99m}Tc-PYP SPECT, enabling reproducible differentiation of ATTR cardiomyopathy; Furuta et al. [24] demonstrated improved SBR and SUR accuracy in ^{123}I-FP-CIT SPECT, reducing SUR error to 6.2%. In radiopharmaceutical therapy, Liu et al. [21] evaluated three PVC methods (RC-PVC, RVC, IY) in ^{177}Lu-PSMA-617 SPECT/CT, with IY and RC-PVC markedly reducing tumor MAE and improving kidney quantification.

Strengths of anatomically-guided post-reconstruction PVC include improved accuracy in standardized uptake metrics (SBR, SUR, RC), reduced quantification error in both phantom and patient data, and enhanced reproducibility in dose mapping. However, performance depends heavily on accurate segmentation and inter-modality registration, and errors in alignment or subject-specific anatomy can degrade correction accuracy. The computational complexity and requirement for high-quality anatomical imaging may limit adoption in resource-constrained settings. Figures 10 and 11 illustrate representative examples from phantom and clinical SPECT datasets, showing how RVC and IY PVC methods improve activity recovery over time across different imaging time points (2–200 h).

Non-anatomically-guided post-reconstruction-based PVC

These techniques correct PVEs using statistical models, blind deconvolution, or RC scaling without relying on structural imaging. Yin and Chiu [26] demonstrated that segmentation-free blind deconvolution with anatomical filtering improved quantification in ^{123}I-mIBG cardiac SPECT/CT without pre-measured PSF. Finocchiaro et al. [22] used phantom-derived RCs to enhance activity estimation in PRRT with ^{177}Lu-labeled analogues, whereas Ramonaheng et al. [237] showed via Monte Carlo simulations that optimized RCs and calibration factors significantly improved ^{177}Lu SPECT accuracy. Azimi et al. [240] applied PVC in ^{177}Lu-PSMA therapy planning, reducing RMSE by 2.83% and improving dose homogeneity.

The appeal of non-anatomical methods lies in simplicity, segmentation independence, and adaptability across tracers

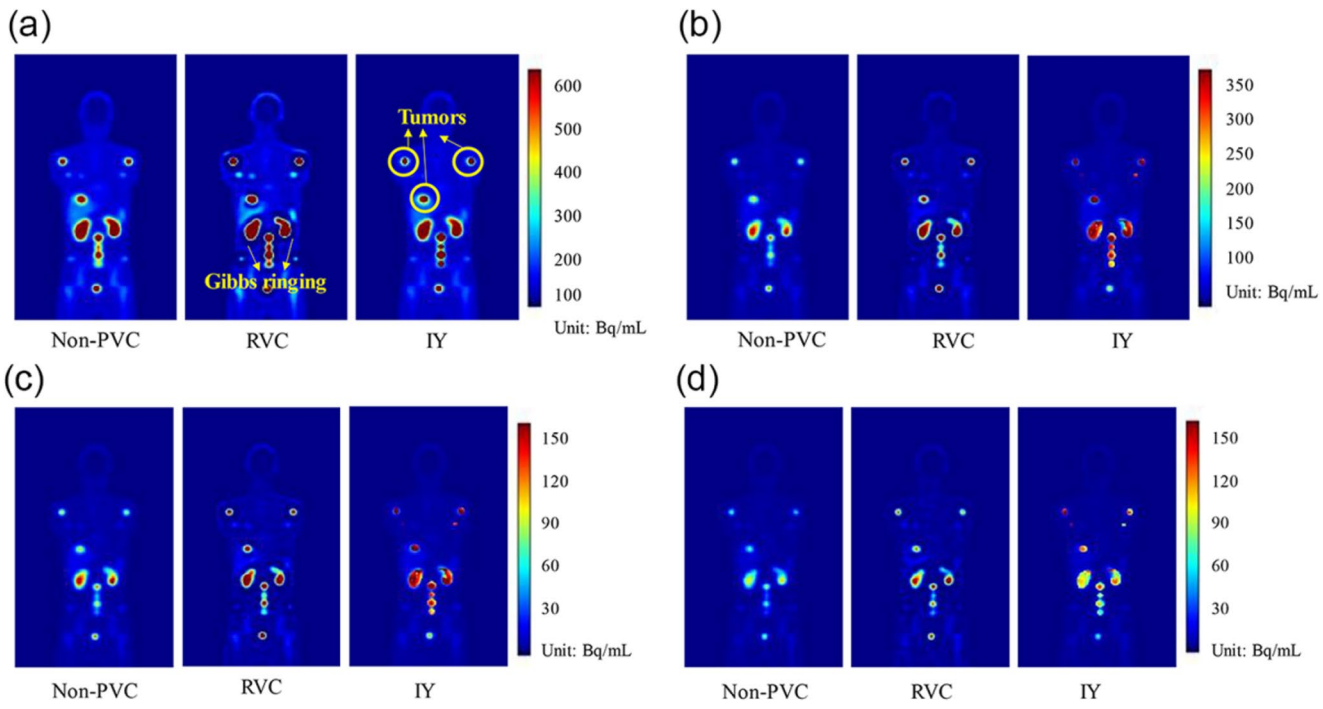

Fig. 10 Representative non-PVC reconstructed images and PVC results (RVC and IY) for an XCAT phantom at four imaging time points: (**a**) 2 h, (**b**) 20 h, (**c**) 40 h, and (**d**) 200 h. The PVC-corrected images show improved activity recovery and clearer delineation of structures compared to non-PVC images, particularly at earlier time points when partial volume effects are more pronounced. Reprinted with permission from [21] under a Creative Commons Attribution License (CC BY 4.0 DEED)

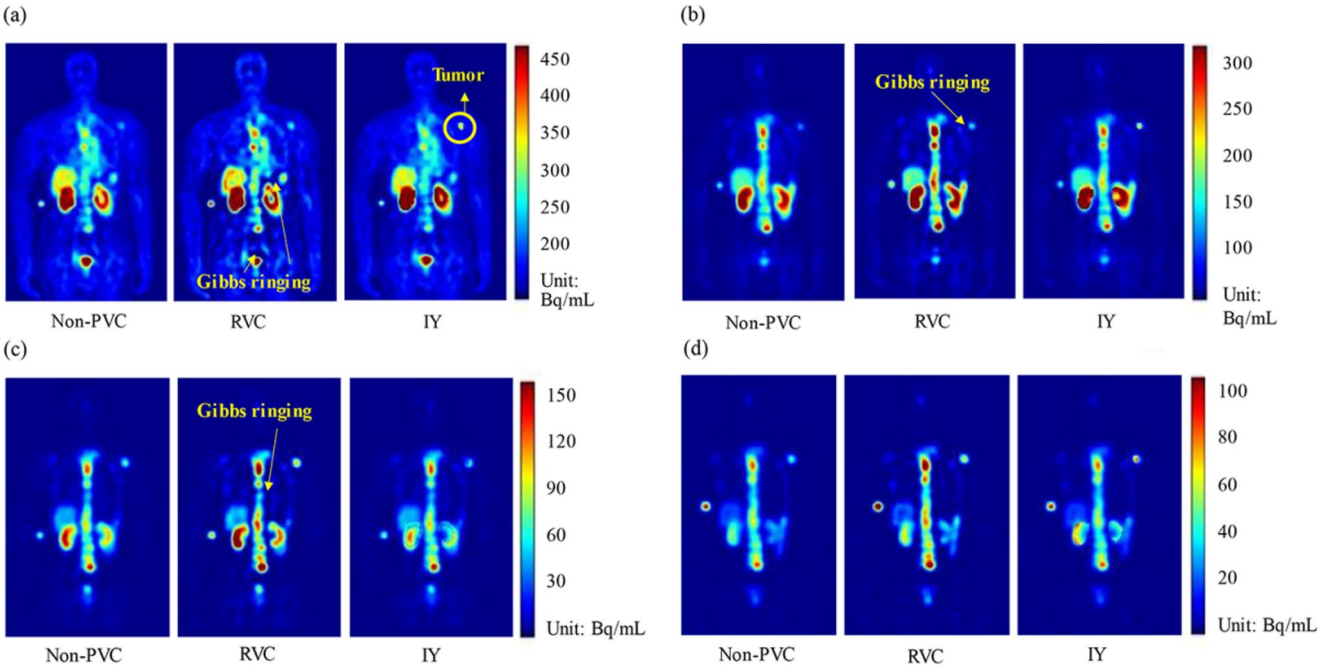

Fig. 11 Representative clinical SPECT images for a patient, with corresponding PVC results (RVC and IY) at (**a**) 2 h, (**b**) 20 h, (**c**) 40 h, and (**d**) 200 h imaging time points. The PVC-corrected images demonstrate enhanced lesion contrast and quantitative accuracy, reducing underestimation of activity evident in non-PVC reconstructions. Reprinted with permission from [21] under a Creative Commons Attribution License (CC BY 4.0 DEED)

and protocols. However, their performance can vary with tracer type, lesion size, noise level, and camera resolution. Without anatomical constraints, they may lack spatial specificity and struggle in heterogeneous or low-contrast regions. Nevertheless, voxel-based and RC-based corrections, particularly in radiopharmaceutical therapy, have shown clear clinical value. As illustrated in Fig. 12, applying PVC to a 2-compartment kidney phantom markedly improves activity concentration and dose distribution profiles, especially at organ boundaries, yielding results that better match nominal reference values.

Hybrid and AI-based PVC in SPECT imaging

The same general concept of hybrid and AI-enhanced PVC applies to SPECT. SPECT-specific applications: Early work has shown promise in combining anatomical priors with AI to improve quantification [23, 242–248]. Representative

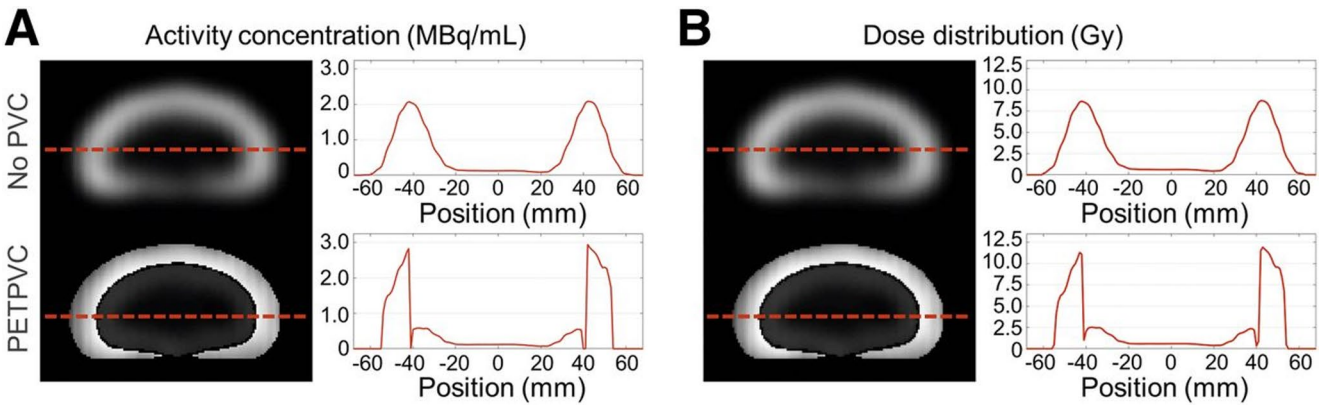

Fig. 12 Effects of partial volume correction (PVC) on quantitative accuracy in molecular radiotherapy. (**A**) Activity concentration maps (MBq/mL) and corresponding line profiles across the kidney phantom before (No PVC) and after PVC. (**B**) Dose distribution maps (Gy) and line profiles for the same cases. Data were reconstructed using Flash3D (48 iterations, 1 subset, 8-mm Gaussian filter). PVC markedly improves boundary definition between compartments, recovers true activity levels, and yields dose distributions that align more closely with nominal reference values, highlighting its clinical relevance for accurate dosimetry. Reprinted with permission from [236] under a Creative Commons Attribution License (CC BY 4.0 DEED)

studies are summarized in Supplementary Table S6. In AI-based PVC, DL approaches have demonstrated encouraging results in SPECT, such as artifact reduction and improved activity recovery in ^{177}Lu SPECT/CT, but these techniques remain experimental and require further validation before routine adoption.

Anatomically-guided hybrid and AI-based PVC

Anatomically-guided hybrid and AI-based PVC methods in SPECT imaging combine the structural specificity of CT/MRI priors with the automation and adaptability of AI algorithms or physics-based modelling. Adam et al. [242] used a 3D-printed phantom to validate a Monte Carlo SPECT-based dosimetry workflow for ^{131}I therapy, refining activity predictions. Yousefi et al. [243] quantified intramyocardial blood volume using ^{99}mTc-RBC SPECT/CT, demonstrating the clinical feasibility of integrating anatomical priors. Salvadori et al. [23] improved kidney activity quantification in ^{177}Lu SPECT through anatomy-based PVC combined with patient-specific segmentation and 3D-printed phantom inserts. As shown in Fig. 13, the process includes segmentation of kidney structures from PET/CT data, CAD-based model design, MSLA 3D printing, and integration into an IEC phantom for validation studies.

These techniques have shown promise in improving spill-out correction in organ-focused applications like kidney and myocardial imaging, where accurate uptake estimation is critical for therapy planning. By reducing reliance on manual processing and enhancing reproducibility, they help standardize quantitative outputs. However, their clinical scalability remains limited by the need for consistently high-quality anatomical inputs, challenges in multimodal registration, and restricted generalizability from narrow training datasets. Without robust multi-centre validation, their wider applicability is still uncertain, though targeted dosimetry use cases appear increasingly well-supported.

Non-anatomically-guided hybrid and AI-based PVC

In contrast, non-anatomically-guided hybrid and AI-based PVC approaches remove the requirement for structural priors by relying on DL models or perturbation-based corrections. Gillen et al. [244] demonstrated improved SPECT quantification using case-specific PSF-based PVC, highlighting the potential of perturbation-guided strategies. Xie et al. [245] proposed a DL-based PVC for cardiac SPECT that required no anatomical guidance, achieving results comparable to anatomically-guided methods and simplifying clinical deployment. Leube et al. [246] developed and validated a deep learning–based PVC method for ^{177}Lu SPECT/CT, trained on Monte Carlo–simulated datasets, which significantly improved activity recovery and spatial accuracy in both simulated and physical phantom experiments (Fig. 14). Wang et al. [247] found that an AttGAN model outperformed U-Net, VC, and non-PVC approaches in reducing noise and improving ^{99}mTc-TRODAT-1 quantification for Parkinson's detection, with clinical results aligning with simulations.

These approaches offer segmentation independence, real-time applicability, and compatibility with diverse tracers. However, clinical translation is challenged by the "black-box" nature of DL, limited interpretability, and a lack of standardized validation pipelines. Performance can vary based on training data diversity and scanner-specific factors. While these models are increasingly central to automated PVC pipelines, broad adoption will require transparent validation, robust generalization, and regulatory readiness.

Discussion, Challenges, limitations and outlook

PVC is widely used in quantitative PET and SPECT imaging to mitigate PVEs, providing not only enhanced tumour detection but also more accurate quantification, including improved SUV/SUVR recovery, reduced small-lesion bias, and more reliable dosimetry, though its effectiveness still varies depending on lesion size, cancer type, and imaging modality [20, 113, 139, 249]. While PVC improves sensitivity, particularly in small lesions, it often reduces specificity and introduces inconsistencies in diagnostic accuracy [164, 168, 184, 185]. In oncology, studies have shown mixed results: PVC enhances tumour detection in head and neck cancers but has limited value in oesophageal cancer [173, 174, 178]. Differences in PVC methodologies, lesion delineation, and biological diversity contribute to these variations [162, 163, 176, 177, 183].

Most oncological PVC applications use simple RC-based methods, which assume spherical tumours with uniform activity distribution. However, these methods are highly sensitive to tumour size estimation errors, leading to biases, either over- or under-estimation, in SUV/SUVR and in absolute quantification [227, 236, 244]. Studies on relapsed/refractory non-Hodgkin's lymphoma show that while PVC improves metabolic activity assessment, it cannot fully correct PVE in small tumours due to spatial resolution limitations [19, 235]. Additionally, iterative deconvolution methods (e.g., Lucy-Richardson) introduce noise and artifacts, reducing clinical feasibility [179, 181, 183]. For longitudinal imaging, errors in PSF modelling, PET-MRI registration, and segmentation propagate through PVC algorithms, degrading accuracy [155, 224, 230, 232]. Despite its promise, PVC struggles with standardization,

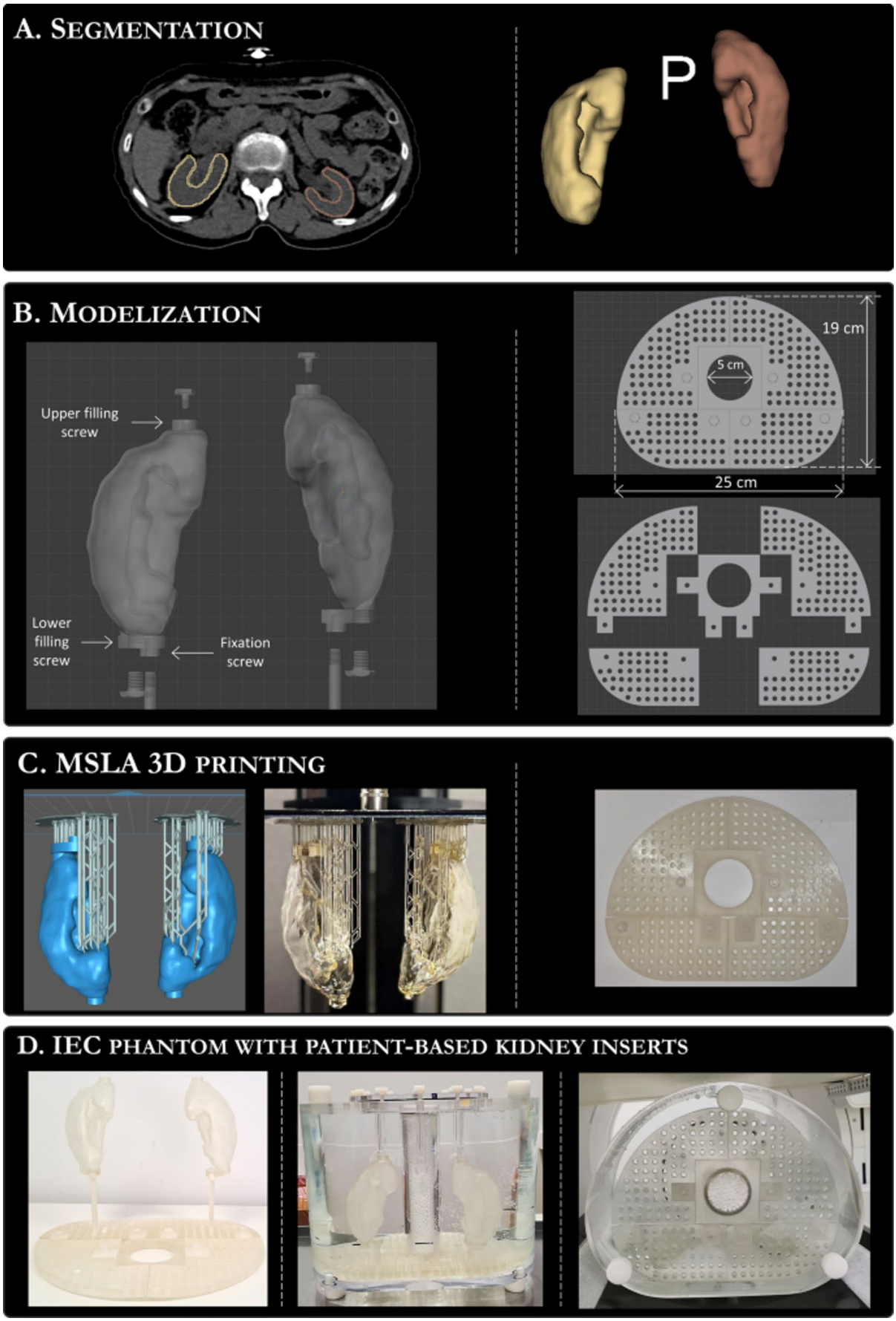
A. SEGMENTATION
P
B. MODELIZATION
Upper filling screw
Lower filling screw
Fixation screw
19 cm
5 cm
25 cm
C. MSLA 3D PRINTING
D. IEC PHANTOM WITH PATIENT-BASED KIDNEY INSERTS

Fig. 13 Workflow for designing and fabricating patient-specific kidney inserts for PVC validation in ^{177}Lu SPECT imaging. Steps start with (**A**) manual segmentation of kidneys from 68Ga-DOTATOC PET/CT scans using 3D-Slicer, followed by (**B**) creation of a modular support system in Blender tailored for IEC phantom integration. (**C**) The kidney inserts and supports are then produced using MSLA 3D printing technology, ensuring anatomical fidelity. (**D**) The final assembly integrates the patient-based inserts into the IEC phantom, enabling realistic evaluation of anatomy-based PVC performance in quantitative imaging studies. Only one representative pair of inserts is shown. Reprinted with permission from [23] under a Creative Commons Attribution License (CC BY 4.0 DEED)

with current methodologies failing to reach a gold standard [234, 237, 242].

Across domains, the value of PVC is task-driven rather than method-specific [177, 181, 188]. In neurology, PVC improves small-structure SUVR/VT and group-level effect sizes when registration and segmentation are robust, especially in regions prone to spill-over (e.g., hippocampus, cortical ribbon) [165, 167–169, 176, 178, 179, 183]. In oncology, benefits concentrate on sub-centimetre lesions and quantitative endpoints (SUV/SUVR, TLG, dosimetry), whereas routine diagnostic gains remain inconsistent across tumour types; size-stratified analyses and protocol harmonisation are essential [181, 182, 184, 185, 188–190, 193]. In cardiology, PVC can refine perfusion and volumetric indices provided PET/SPECT–CT alignment and motion control are reliable [220–222, 226, 230]. These distinctions underscore aligning PVC choice, QC steps, and decision thresholds with the intended clinical endpoint. While both PET and SPECT suffer from PVEs, the nature and severity of PVEs differ between the modalities. PET generally offers higher spatial resolution and improved sensitivity, while SPECT is more prone to scatter and collimator-related distortions, with PVE remains a major source of error in Lu-177 SPECT/CT, particularly for structures smaller than approximately three times the system's FWHM. Consequently, PVC strategies optimized for PET may not directly translate to SPECT and vice versa. The implications for resolution modelling, noise propagation, and algorithmic robustness must be considered modality-specific. In SPECT imaging, PVE is more pronounced due to lower spatial resolution, making PVC potentially more impactful for cardiac imaging, dosimetry, and small lesion quantification [21–23]. Advanced PVC techniques, such as blood-concentration-based and iterative MTC, improve quantification accuracy but remain computationally intensive [24–26]. Some studies show that GTM and RBV increase group separation but also introduce noise and repeatability issues [209, 243, 246]. DL approaches like DeepPVC have improved processing speed, but their accuracy in small brain regions remains inferior to conventional methods [205, 214–216]. Additionally, in ^{99m}Tc-tetrofosmin

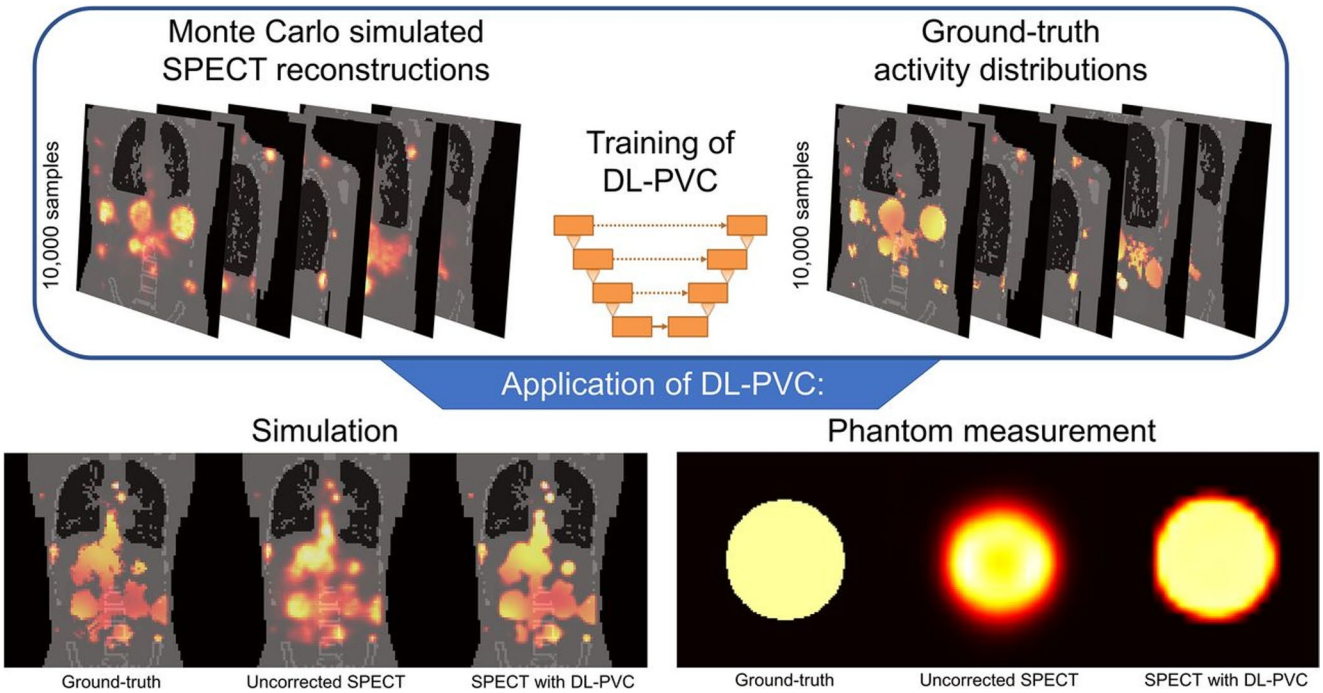

Fig. 14 Workflow and results of the deep learning–based PVC (DL-PVC) method for ^{177}Lu SPECT/CT imaging. The upper panel shows Monte Carlo–simulated SPECT reconstructions and corresponding ground-truth activity distributions used to train the DL-PVC model with 10,000 samples. The lower panel demonstrates the application of the trained model, comparing ground-truth data, uncorrected SPECT, and DL-PVC–corrected images in both simulation and physical phantom measurements. DL-PVC substantially improves activity recovery and spatial accuracy, especially in small or high-contrast structures. Reprinted with permission from [246] under a Creative Commons Attribution License (CC BY 4.0 DEED)

SPECT, PVC reduced activity bias in perfusion defects, but CT-SPECT misalignment remained a limitation [220–222, 243, 244].

Current evidence does not justify universal, across-the-board use of PVC in routine PET and SPECT imaging. Instead, we advocate a standardised, task-aligned workflow: (i) harmonised acquisition/reconstruction protocols and explicit PSF modelling across centres and vendors (as promoted by EARL accreditation), (ii) validation using shared digital/physical phantoms and recovery-coefficient–based, size-stratified analyses, (iii) consensus guidelines for segmentation and registration per organ/lesion, with integrated QC steps, and (iv) publicly available, annotated datasets and phantom studies for benchmarking and reproducibility [24, 31, 58, 144, 165, 179, 222, 238]. Corrected and uncorrected readouts should be reported side by side with endpoint-specific thresholds, with PVC generally recommended when the target structure is smaller than 2–3 times the system's FWHM (i.e., ≤ 10–15 mm in PET and ≤ 15–25 mm in SPECT), noting that full recovery is rarely achieved for sub-millilitre volumes, underscoring persistent limitations of PVC for very small structures, and therefore, lesions ≤ 10 mm should be excluded from quantitative analyses unless validated PVC is available [199, 249]. For broad clinical adoption, implementations must be simpler, robust, and fast, preferably reconstruction-integrated or well-validated PET-only pipelines with explicit QC for registration and motion, so that bias–variance trade-offs are controlled and results remain reproducible [250–252]. These steps align with ongoing quantitative imaging harmonisation initiatives from SNMMI/EANM procedure standards and theranostic dosimetry guidance endorsing harmonised PVC, including the EANM Research Ltd. (EARL) accreditation program, which sets performance standards and harmonised PET/CT reconstruction protocols to ensure cross-centre comparability and reproducibility [253–256].

While Marquis et al. [51] introduced anatomically-informed RC models that significantly improved mean quantification accuracy in PET/SPECT, their evaluation framework did not assess precision or robustness under varying conditions. Reliability and generalizability of such PVC methods remain to be thoroughly investigated, and performances of such correction strategies, and associated software tools, may be task-specific and require validation for different clinical scenarios.

The use of PVC in SPECT imaging is somewhat distinct, with Perturbation-based GTM (pGTM) as an approach of good potential for PVC [42]. This method is particularly effective in addressing Gibbs artifacts in low-resolution systems like SPECT with parallel-hole collimators. In cardiac SPECT, PVC has proven valuable for improving myocardial perfusion imaging, enabling clearer visualization of ischemic regions and scars. However, significant challenges persist, including resolution mismatches and registration errors between CT and SPECT, leading to inaccuracies in parameters like intramyocardial blood volume (IMBV). Moreover, signal spillover in small or boundary regions often remains uncorrected, and in some cases, differential methods result in negative voxel values. Anatomical structures like myocardial walls or ventricular blood in non-contrast CT scans may be poorly distinguished, impacting PVC accuracy. While anatomy-based methods have shown promise in voxel-based dosimetry, precise image reconstruction and correction of PVE remain critical for improved estimates. Emerging techniques, such as DL-based PVC, have demonstrated encouraging results in applications like ^{177}Lu SPECT/CT, offering artifact correction and improved activity recovery [246]. However, these approaches are still experimental, requiring further development for routine clinical use. The future of PVC in SPECT imaging lies in developing larger disease-specific datasets, standard evaluation metrics, and seamless integration of advanced correction tools into clinical workflows. The structure of Table 1 reflects the categorization of PVC studies based on imaging modality (PET, SPECT, or both) and clinical focus. While several pitfalls and challenges, such as segmentation inaccuracies, noise amplification, or dependency on high-resolution anatomical imaging, are inherently relevant to both PET and SPECT, they are allocated here according to the primary modality focus in the reviewed studies. This facilitates a comparative view of method-specific advantages, technical barriers, and translational prospects.

Post-reconstruction PVC can improve recovery but often amplifies mid-frequency noise (e.g., RL ringing) and remains vulnerable to PET–anatomy misregistration and segmentation variability. GTM/RBV may elevate noise and struggle with complex signals and small regions, while MG/SGTM depend heavily on high-quality MRI and accurate tissue labelling. Parallel level set (PLS) approaches likewise introduce risks of over-smoothing or instability in heterogeneous regions. More practical implementations therefore combine deconvolution with advanced denoising, integrate respiratory/cardiac or data-driven motion correction, and apply automated checks to mitigate registration or segmentation errors. Minimising manual VOI delineation remains critical to reduce operator dependence and variability. Taken together, these safeguards are essential if post-reconstruction PVC methods are to become reliable and reproducible enough for routine clinical adoption [107, 144, 179, 200].

From a clinical perspective, only a limited subset of PVC methods, most notably PSF-integrated reconstruction techniques, are currently adopted in routine clinical workflows, as they are embedded in commercial PET and SPECT software. Other methods, including anatomically guided

Table 1 Summary of the benefits, pitfalls, challenges, limitations, and future outlook of studies focusing on PVC in PET and SPECT imaging systems. Rows are grouped by imaging modality and clinical domain (e.g., oncology, neurology, therapy planning)

Modality	Benefits	Pitfalls	Challenges	Outlook
PET	Enhances sensitivity for smaller lesions and improves treatment response prediction in cancers such as head and neck.	Reduced specificity and inconsistent improvement in diagnostic accuracy unless SUV/SUVR thresholds are appropriately adjusted.	Lack of standardized PVC protocols and inconsistencies in lesion delineation.	Development of DL-based PVC (e.g., DeepPVC) holds promise but requires further optimization for small regions.
	Improves accuracy of kinetic parameters like VT and BPND, aligning them with SUV and TBR.	Post-reconstruction PVC methods introduce artifacts such as Gibbs ringing and edge overshoot, and noise amplification limits the clinical applicability of iterative deconvolution methods (e.g., Lucy–Richardson).	Misregistration between PET and MRI reduces alignment accuracy for GTM and MG-based PVC methods.	AI advancements, including FastPET and diffusion models, show potential to overcome PVC challenges.
	Enhances quantification in amyloid and tau studies with reduced signal spill-in/spill-out using RBV techniques.	Limited impact on lesions ≤ 10 mm due to segmentation inaccuracies and noise amplification, with PVC benefits diminishing in longitudinal studies due to added noise and potential data distortion.	High dependency on accurate PSF modelling and segmentation precision.	Emerging hardware (e.g., LAFOV scanners) could address PVE challenges in multi-organ studies.
	Shows utility in early disease detection (e.g., Huntington's disease gene carriers) by capturing metabolic changes.	High dependency on high-resolution anatomical information (e.g., MRI or CT) and segmentation accuracy, with no clear gold standard for method comparison; MRI-based PVC used as a reference remains imperfect.	Limited generalizability of DeepPVC due to reliance on tracer-specific features.	Research should prioritize harmonizing PET-MRI data integration and optimizing DL-PVC for multi-task applications.
SPECT	Improves quantitative accuracy in myocardial perfusion imaging and dosimetry, especially for small objects.	Post-reconstruction PVC methods amplify noise and struggle with spill-over correction in small or boundary regions, particularly in low-resolution systems.	Alignment issues between CT and SPECT reduce accuracy in hybrid imaging.	Deep learning (e.g., DL-PVC) and Monte Carlo simulations hold potential for improving PVC in SPECT.
	Reduces errors in myocardial blood volume (IMBV) estimates and enhances dose differentiation in kidney imaging.	Overcorrection by PVC may lead to overestimated specific binding ratios (SBR) in some cases, and current methods often fail to fully correct PVE in non-uniform tissue distributions or small anatomical structures.	Voxel-level dosimetry for anisotropic SPECT resolution requires optimization and adaptation; full recovery is rarely achieved for sub-mL volumes, underscoring limitations in very small structures.	Automating segmentation processes and adapting PVC methods for fast-paced clinical workflows are key.
	Advanced PVC methods like RGTM improve accuracy in challenging conditions (e.g., small nucleus accumbens regions).	PSF modelling often assumes spatial invariance, overlooking motion-related or system-induced variations, and noise/artifacts (e.g., Gibbs) remain significant obstacles in fast clinical workflows.	Computationally intensive segmentation and motion artifacts hinder clinical adoption.	Standardizing calibration and recovery factors across centers can enhance reproducibility and utility.
	Enhances spatial resolution and signal differentiation in SPECT imaging (e.g., with methods like SPECTRE).	Dependence on high-resolution CT for anatomical guidance limits routine clinical use; absence of commercial PVC software and computational intensity hinder broader adoption.	Errors in segmentation and resolution mismatches between CT and SPECT reduce quantification accuracy.	Validation of advanced methods like DL-PVC and multi-resolution modelling can pave the way for clinical adoption.
PET/SPECT	Enhances dosimetry accuracy in radionuclide therapies such as Lu-177 theranostics, improving personalized treatment planning and therapeutic monitoring by reducing PVE-related errors, which are particularly pronounced for structures $< 3\times$FWHM	Lack of standard evaluation metrics and high dependency on high-resolution anatomical imaging (e.g., MRI or CT), particularly in radiotherapy planning (RTP), limit consistent application; such imaging may not always be available, reducing reproducibility and clinical reliability.	The need for standardized and reproducible PVC methods remains a key challenge, as no clear gold standard exists for method comparison, and most current evidence is still phantom-based with limited patient validation.	Deep learning models like DeepPVC, FastPET, and diffusion models show promise but still require optimization and validation across different tracers. Personalized dosimetry in theranostics (e.g., Lu-177, Tb-161) is an emerging application.

Table 1 (continued)

Modality	Benefits	Pitfalls	Challenges	Outlook
PET/SPECT	Enhances delineation of PTV and BTV by reducing PVE, leading to better dose distribution and improved tumor targeting	Increased computational complexity and dependency on segmentation accuracy may introduce errors in volume definition, while heterogeneous tracer uptake (e.g., due to perfusion changes) can reduce the accuracy of anatomy-based methods.	Standardization of PVC algorithms for RTP remains a challenge, as different correction methods may yield variable outcomes; generalizability across scanners, tracers, and protocols remains limited.	Integration of AI-driven PVC methods with adaptive radiotherapy planning could optimize treatment personalization and dose accuracy.

approaches (e.g., PETPVC) and AI-driven or voxel-wise techniques, are still predominantly used in research settings due to limited validation and lack of regulatory approval. These distinctions are reflected in Table 2 and illustrated in Figure S1, which provide an overview of the clinical readiness and translational maturity of various PVC methods.

While advancements in DL offer promise for PVC without anatomical data, these methods are still in early stages and require extensive validation. Looking ahead, hardware advancements, especially the emergence of long axial field-of-view (LAFOV) PET/CT scanners, such as the uEXPLORER, PennPET Explorer, and Biograph Vision Quadra, have shown strong potential in addressing PVE challenges [257]. These systems provide dramatically higher sensitivity, improved lesion detectability, and the capability for comprehensive (e.g., whole-body) imaging protocols without bed translation. For example, the uEXPLORER offers up to 15–68× higher sensitivity compared to conventional PET, while both PennPET Explorer and Biograph Vision Quadra demonstrated improved signal-to-noise ratios and spatial resolution, enabling lower-dose or faster scans [258]. Studies by Mannheim et al. [259] have shown significant variations in PVE across the FOV, driven by object size, signal-to-background ratio, and isotope type, with contrast recovery coefficient (CRC) differences reaching up to 50%. These findings underscore the importance of accounting for FOV-dependent PVE variability in clinical interpretations, particularly in multi-organ or dynamic studies. Furthermore, the increasing use of novel radiopharmaceuticals, such as ^{161}Tb, ^{177}Lu, and ^{225}Ac theranostic agents used for radiopharmaceutical therapies, will likely require adapted PVC methods that account for their unique spatiotemporal biodistributions. Future research should explore how radiopharmaceutical properties interact with resolution effects and impact the optimization of PVC algorithms.

Looking ahead, AI holds significant promise in addressing the limitations of PVC. For instance, Panin et al. introduced the FastPET network, which uses compressed TOF data as input to reconstruct high-quality PET images without blurring [260]. This approach, referred to as reconstruction-based PVC, represents a much-needed advancement, combining PVC with AI to deliver enhanced resolution and speed. While early results are promising, further research and clinical validation are necessary to fully realize its potential. Similarly, DL methods and diffusion models offer hope for the future, potentially enabling PVC to become a routine clinical tool, tailored to the specific requirements of each task. PVC-specific standardization is still lacking; however, future integration with broader SNMMI/EANM harmonization efforts may provide the framework needed for clinical validation [261]. Meanwhile, recent AI-based approaches have begun to address issues like noise sensitivity and limited generalizability, though further validation remains necessary [61].

Despite these promising efforts, it is important to recognize several outstanding challenges. AI-based PVC methods often require large, diverse, and well-annotated datasets, which are not always available [215]. Moreover, models trained on one type of scanner, population, or protocol may not generalize well to others, leading to performance variability [262]. The "black box" nature of DL also limits interpretability, making it difficult for clinicians and regulators to understand the rationale behind corrections, thereby affecting trust and adoption in clinical settings [263].

To further support our analysis, Figure S1 illustrates a comparative assessment of clinical readiness across 11 common PVC methods based on literature-reported evidence of their deployment, reliability, and feasibility. Additionally, Figure S2 provides a side-by-side comparison of SUV_{max} changes across different PVC techniques in typical brain and oncology imaging settings, highlighting variability in signal recovery and emphasizing the context-specific nature of each method's effectiveness. These visualizations aim to complement the tabulated summaries by offering a clearer overview of method-specific trends and performance characteristics across modalities.

Bridging the gap between research and clinical practice requires a multidisciplinary approach, focusing on the development of robust and efficient PVC methods, simplifying segmentation processes, and validating these techniques on larger, more diverse clinical datasets. Collaboration between imaging experts, clinicians, and machine learning researchers could accelerate the integration of PVC into routine clinical workflows. With these efforts, PVC can

Table 2 Comparative overview of commonly used PVC methods in PET and SPECT, including methodology, strengths, limitations, clinical potential, and implementation resources (open-source tools, pipelines, github repositories)

Method	Open-Source Implementation/Tools	Benefits	Pitfalls	Mainly Applied to (Organ/Tissue)	Will It be Routinely Deployed in the Clinic?
Point Spread Function (PSF)	PETPVC Toolbox	Improves internal signal reconstruction accuracy Reduces need for post-reconstruction corrections	Sensitive to spatial resolution variations Limited in handling complex datasets	Brain, cardiac, oncology (General PET/SPECT)	Definitely yes (already deployed)
Recovery Coefficient (RC)	MIRDPVC	Simple and quick for initial calculations Effective for small and spherical lesions	Typically assumes uniform activity distribution Sensitive to tumour size estimation errors High noise and artifacts	Tumours (oncology PET/SPECT, small lesions, radiopharmaceutical dosimetry)	Most likely yes
Deep Learning-based (DL)	Implemented in specific research studies; not publicly available	Faster processing Advanced noise removal and signal correction Scalable to large datasets	Requires large datasets for training Challenges in generalization to various data types Limited for small regions	Brain, cardiac, oncology (multi-tracer PET/SPECT, General PET/SPECT). emerging applications	Most likely yes
Region-Based Voxelwise (RBV)	PETPVC Toolbox	Reduces extracortical noise Effective for correcting signals in small regions	Overemphasizes cortical signals Limited accuracy in group-level statistical analyses	Brain (cortex/hippocampus, Alzheimer's, tau/small structures)	Most likely yes
Perturbation-based GTM (pGTM)	Implemented in specific research studies; not publicly available	Reduces Gibbs artifacts Effective in low-resolution systems like SPECT	Requires precise modelling Sensitive to structural misalignments and noise	Heart (SPECT MPI), tumours (oncology SPECT)	Most likely yes
Iterative Deconvolution	PETPVC Toolbox	Effective in reducing spill-over and spill-in effects Useful for high-resolution reconstructions	Amplifies noise in dynamic datasets Computationally expensive Limited clinical standardization	Brain, tumours, (General PET/SPECT)	Most likely yes (Research-focused)
Geometric Transfer Matrix (GTM)	PETPVC Toolbox	High accuracy in reducing partial volume effects Suitable for longitudinal studies	Requires precise PET/MRI registration Sensitive to structural changes like brain atrophy Increases noise	Brain (cortical regions, longitudinal neuroimaging, Alzheimer's)	Most likely yes(Research-focused)
Iterative Yang (IY)	PETPVC Toolbox	Suitable for iterative reconstructions Reduces noise in dynamic images	Computationally intensive Introduces noise and artifacts under certain conditions	Brain (dynamic PET), cardiac (SPECT MPI), small tumours	Unlikely (primarily for research)
Parallel level set (PLS)	Implemented in specific research studies; not publicly available	Better quantification in small cortical regions (e.g., amyloid/tau PET).	Requires high-quality MRI segmentation/registration	Brain (amyloid/tau PET, cortical imaging), small tumours (oncology PET). MRI-guided, mainly brain PET	Unlikely (Primarily research-focused)

Table 2 (continued)

Method	Open-Source Implementation/Tools	Benefits	Pitfalls	Mainly Applied to (Organ/Tissue)	Will It be Routinely Deployed in the Clinic?
Müller-Gärtner (MG)	PETPVC Toolbox	Effective for brain signal correction in Alzheimer's patients Compatible with longitudinal approaches	Highly dependent on PET/MRI alignment Susceptible to segmentation errors	Brain (Alzheimer's, cortical imaging, hippocampus)	Unlikely (primarily for research)
Blind Deconvolution (BD)	Implemented in specific research studies; not publicly available	Reduces noise without prior PSF knowledge; improves contrast.	Requires simultaneous PSF estimation; prone to errors with motion artifacts or noisy datasets.	General PET/SPECT, small tumours (research-focused)	Unlikely (primarily for research)
SPECTRE	Implemented in specific research studies; not publicly available	Improves spatial resolution Enhances signal differentiation Effective in oncology imaging	Computationally demanding Susceptible to scatter correction and image misalignment challenges	Tumours (oncology SPECT, bone metastases, radiopharmaceutical therapy dosimetry)	Unlikely (primarily for research)

evolve into a critical tool for enhancing diagnostic precision and personalizing patient care, paving the way for a more accurate and efficient clinical paradigm. Table 2 provides a comparative overview of commonly used PVC methods in PET and SPECT imaging, including their strengths, limitations, and potential for adoption in clinical workflows, while Fig. 15 graphically summarizes their relative likelihood of routine clinical use.

Conclusion and future perspectives

Based on the available evidence, PVC can be either beneficial or detrimental depending on the specific task, and we cannot and should not assert its effectiveness categorically across all applications. For instance, while PVC improves quantification in small lesions, it may also amplify noise or introduce segmentation-induced bias and artifacts in

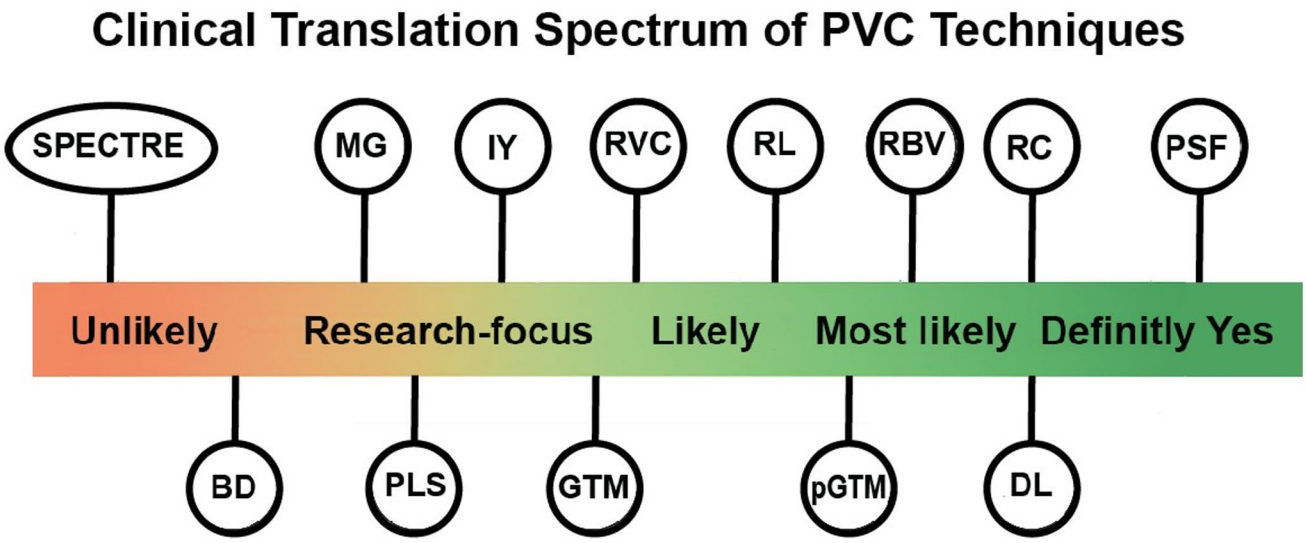

Fig. 15 Graphical summary of the clinical readiness of partial volume correction (PVC) methods. PVC methods are positioned along a spectrum from unlikely to definitely yes regarding their likelihood of routine clinical adoption. This figure provides a visual overview to complement the detailed comparative information presented in Table 2

complex or heterogeneous regions, thereby reducing interpretability or diagnostic confidence. What is clear, however, is that while various PVC methods exist, they have not yet been widely adopted as practical tools in clinical practice. By "widely adopted", we refer to their integration into standardized clinical workflows, inclusion in vendor-supported software, and use in multi-centre trials. Moreover, validated software for post-reconstruction PVC methods is not widely adopted by industry, limiting standardization and broader clinical implementation. These methods face numerous challenges, including computational complexity and time consumption, sensitivity to noise, reliance on accurate image registration, lack of generalizability, difficulties with small structures and uptake heterogeneity, advancements in reconstruction-based approaches like PSF, and cost and equipment limitations.

In contrast, reconstruction-based methods, such as PSF modelling, are now widely implemented on modern PET and SPECT systems. These methods address PVEs inherently during the reconstruction process, reducing the need for separate post-reconstruction PVC corrections. While DL-based models have shown promising results, in task-specific image evaluations, there are still significant barriers to the clinical translation of AI tools, and the number of studies in this area remains limited. However, these methods are rapidly evolving, and we are optimistic about their potential to become more effective and support existing approaches in the future. Ultimately, this review synthesizes findings across more than 150 articles and identifies context-specific advantages of PVC techniques across neurological, oncological, and cardiac applications.

As a result, there is an urgent need for large disease-specific datasets, standardized and reproducible PVC approaches, and integration of advanced image enhancement tools into existing clinical workflows. These efforts will be crucial for the successful adoption and clinical implementation of both PVC and AI-driven methods. Finally, while PVC methods have clear potential, their application must be context-aware, evidence-driven, standardized, and reproducible to ensure reliable clinical integration.

Abbreviations

PET	Positron Emission Tomography
SPECT	Single–Photon Emission Computed Tomography
CT	Computed Tomography
MRI	Magnetic Resonance Imaging
PVE	Partial Volume Effect
PVC	Partial Volume Correction
FWHM	Full Width at Half Maximum
FOV	Field of View
PSF	Point Spread Function
RBV	Region–Based Voxel–wise
GTM	Geometric Transfer Matrix
RC	Recovery Coefficient
SGTM	Simplified Geometric Transfer Matrix
MG	Müller–Gärtner
pGTM	Perturbation–Based Geometric Transfer Matrix
IDM	Iterative Deconvolution Model
IY	Iterative Yang
RL	Richardson–Lucy Deconvolution
RVC	Reblurred Van Cittert
PLS	Parallel Level Set
BD	Blind Deconvolution
SFSRR	Structural–Functional Synergistic Resolution Recovery
STC	Single–Target Correction
TOF	Time–of–Flight
QC	Quality Control
FBP	Filtered Back–Projection
SNR	Signal–to–Noise Ratio
MAE	Mean Absolute Error
RMSE	Root Mean Square Error
MPI	Myocardial Perfusion Imaging
SBR	Specific Binding Ratio
ICC	Intraclass Correlation Coefficient
COV	Coefficient of Variation
SSIM	Structural Similarity Index
PSNR	Peak Signal–to–Noise Ratio
CRC	Contrast Recovery Coefficient
SUV	Standardized Uptake Value
TBR	Tumour–to–Background Ratio
VT	Distribution Volume
BPND	Binding Potential Non–Displaceable
IMBV	Intramyocardial Blood Volume
TLG	Total Lesion Glycolysis
HMR	Heart–to–Mediastinum Ratio
SUR	Specific Uptake Ratio
DL	Deep Learning
AI	Artificial Intelligence
CNN	Convolutional Neural Network
DeepPVC	Deep Learning–Based Partial Volume Correction
CycleGAN	Cycle–Consistent Generative Adversarial Network
FastPET	AI–Based PET Image Reconstruction Model
DL	PVC–Deep Learning–Based Partial Volume Correction
SUVR	Standardized Uptake Value Ratio
^{18}F	FDG–Fluorodeoxyglucose, a PET radiotracer
^{11}C	PiB–Pittsburgh Compound B, used in amyloid imaging

^{18}F	AV1451–Tau PET imaging tracer
^{18}F	Flutemetamol–PET tracer for amyloid imaging
^{99m}Tc	Technetium–99 m, a common SPECT radiotracer
^{177}Lu	Lutetium–177, used in radionuclide therapy
^{131}I	Iodine–131, used in thyroid and radiotherapy imaging
^{99m}Tc	PYP–Technetium–99 m Pyrophosphate, used in cardiac imaging
^{99m}Tc	RBC–Technetium–99 m Red Blood Cell Labelling
^{68}Ga	DOTATOC–Gallium–68 DOTATOC, used in neuroendocrine tumour imaging
^{18}F	MK–6240–PET tracer for tau pathology
^{11}C	UCB–J–Synaptic Vesicle Glycoprotein 2 A tracer
^{18}F	NaF–Sodium Fluoride
^{123}I	FP–CIT–DaT tracer
^{123}I	mIBG–Meta–Iodobenzylguanidine
^{99m}Tc	TRODAT–1–DaT SPECT tracer
^{124}I/^{131}I	CLR1404–Alkylphosphocholine theranostic
^{11}C	FMZ–Flumazenil
^{161}Tb	Terbium–161
^{225}Ac	Actinium–225
NSCLC	Non–Small Cell Lung Cancer
PSMA	Prostate–Specific Membrane Antigen
HNSCC	Head and Neck Squamous Cell Carcinoma
AD	Alzheimer's Disease
MCI	Mild Cognitive Impairment
DAT	Dopamine Transporter
MAO	B–Monoamine Oxidase B
LAFOV	Long Axial Field–of–View
OSEM	Ordered Subset Expectation Maximization
HYPR	HighlY constrained backPRojection
ROI	Region of Interest
VOI	Volume of Interest
PTV	Planning Target Volume
BTV	Biological Tumor Volume
RTP	Radiotherapy Planning
ATTR	Transthyretin Amyloidosis
AMAP	S / AMAP–R–Anatomically–guided Maximum A–Posteriori
PETPVC	PET Partial Volume Correction toolbox
APPIAN	Automated Pipeline for PET Image Analysis
HC	Healthy Controls
SNMMI	Society of Nuclear Medicine and Molecular Imaging
EANM	European Association of Nuclear Medicine
EARL	EANM Research Ltd. (Accreditation Program)

Supplementary Information The online version contains supplementary material available at https://doi.org/10.1007/s00259-025-07612-5.

Author contributions MSA: Conceptualization, Methodology, Formal analysis, Investigation, Resources, Writing – original draft, Writing – review & editing, Visualization. HA, AS, NZ, YB, CL, AA, MK, RB: Conceptualization, Methodology, Validation, Investigation, Writing – review & editing, Visualization. AR, HZ: Conceptualization, Methodology, Validation, Investigation, Resources, Writing – review & editing, Supervision, Project administration, Funding acquisition.

Funding This work was supported by the Swiss National Science Foundation under grant SNSF 320030−231742 and the BC Cancer Foundation.

Data availability The data used in this work is not available.

Declarations

Ethical approval All procedures performed in studies involving human participants were in accordance with the ethical standards of the institutional and/or national research committee and with the 1964 Helsinki declaration and its later amendments or comparable ethical standards.

Consent to participate NA.

Consent to publish All authors approved the final version of the manuscript and consent to give the Publisher the permission to publish the work.

Competing interests Prof. Zaidi received funding from General Electric Healthcare not related to the present manuscript. Dr. Navid Zeraatkar is currently a full-time employee of Siemens Medical Solutions, Inc. USA. The other authors have nothing relevant to declare.

References

1. Hoffman EJ, Huang S-C, Phelps ME. Quantitation in positron emission computed tomography: 1. Effect of object size. J Comput Assist Tomogr. 1979;3:299–308.
2. Hoffman EJ, Huang S-C, Plummer D, Phelps ME. Quantitation in positron emission computed tomography: 6. effect of nonuniform resolution. J Comput Assist Tomogr. 1982;6:987–99.
3. Basu S, Hess S, Braad P-EN, Olsen BB, Inglev S, Høilund-Carlsen PF. The basic principles of FDG-PET/CT imaging. PET Clin. 2014;9:355–70.
4. Hussain S, Mubeen I, Ullah N, Shah SSUD, Khan BA, Zahoor M, et al. Modern diagnostic imaging technique applications and risk factors in the medical field: a review. BioMed Res Int. 2022;2022:5164970.
5. Blomberg BA, Bashyam A, Ramachandran A, Gholami S, Houshmand S, Salavati A, et al. Quantifying [^{18}F]fluorodeoxyglucose uptake in the arterial wall: the effects of dual time-point imaging and partial volume effect correction. Eur J Nucl Med Mol Imaging. 2015;42:1414–22.
6. Pretorius PH, King MA. Diminishing the impact of the partial volume effect in cardiac SPECT perfusion imaging. Med Phys. 2009;36:105–15.
7. Kessler RM, Ellis JR Jr, Eden M. Analysis of emission tomographic scan data: limitations imposed by resolution and

background. J Comput Assist Tomogr. 1984. https://doi.org/10.1097/00004728-198406000-00028.
8. Rahmim A, Zaidi H. PET versus SPECT: strengths, limitations and challenges. Nucl Med Commun. 2008;29:193–207.
9. Lu F-M, Yuan Z. PET/SPECT molecular imaging in clinical neuroscience: recent advances in the investigation of CNS diseases. Quant Imaging Med Surg. 2015;5:433.
10. Soret M, Bacharach SL, Buvat I. Partial-volume effect in PET tumor imaging. J Nucl Med. 2007;48:932–45.
11. Cherry SR, Sorenson JA, Phelps ME. ScienceDirect. Physics in nuclear medicine. Soc Nuclear Med; 2003.
12. Rousset OG, Ma Y, Evans AC. Correction for partial volume effects in PET: principle and validation. J Nucl Med. 1998;39:904–11.
13. Rousset O, Rahmim A, Alavi A, Zaidi H. Partial volume correction strategies in PET. PET Clin. 2007;2(2):235–49.
14. Picard Y, Thompson CJ. Motion correction of PET images using multiple acquisition frames. IEEE Trans Med Imaging. 1997;16:137–44.
15. Schäfers K, Dawood M, Lang N, Büther F, Schäfers M, Schober O. Motion correction in PET/CT. Nuklearmedizin-NuclearMedicine. 2005;44:S46-50.
16. Kovalski G, Israel O, Keidar Z, Frenkel A, Sachs J, Azhari H. Correction of heart motion due to respiration in clinical myocardial perfusion SPECT scans using respiratory gating. J Nucl Med. 2007;48:630–6.
17. Catana C. Motion correction options in PET/MRI. Seminars in nuclear medicine. Elsevier; 2015; pp. 212–23.
18. Pretorius PH, Johnson KL, Dahlberg ST, King MA. Investigation of the physical effects of respiratory motion compensation in a large population of patients undergoing Tc-99m cardiac perfusion SPECT/CT stress imaging. J Nucl Cardiol. 2020;27:80–95.
19. Wu J, Liu C. Recent advances in cardiac SPECT instrumentation and imaging methods. Phys Med Biol. 2019;64:06TR01.
20. Nguyen T, Høilund-Carlsen PF, Zaidi H, Vach W. Clinical relevance of partial-volume effect: dependence on lesion size and shape. IEEE nuclear science symposium and medical imaging conference (NSS/MIC). Atlanta, USA: IEEE; 2017. pp. 1–2.
21. Liu Y, Lu Z, Chen G, Shi K, Mok GS. Partial volume correction for Lu-177-PSMA SPECT. EJNMMI Phys. 2024;11:93.
22. Finocchiaro D, Berenato S, Grassi E, Bertolini V, Castellani G, Lanconelli N, et al. Partial volume effect of SPECT images in PRRT with ^{177}Lu labelled somatostatin analogues: a practical solution. Phys Med. 2019;57:153–9.
23. Salvadori J, Allegrini O, Opsommer T, Carullo J, Sarrut D, Porot C, et al. Anatomy-based correction of kidney PVE on 177 Lu SPECT images. EJNMMI Phys. 2024;11:15.
24. Furuta A, Onishi H, Yamaki N, Yada N, Amijima H. Impact of quantitative index derived from 123I-FP-CIT-SPECT on reconstruction with correction methods evaluated using a 3D-striatum digital brain phantom. Radiol Phys Technol. 2018;11:294–302.
25. Pourmoghaddas A, Wells RG. Quantitatively accurate activity measurements with a dedicated cardiac SPECT camera: physical Phantom experiments. Med Phys. 2016;43:44–51.
26. Yin T-K, Chiu N-T. Correction of partial volume effect in 99mTc-TRODAT-1 brain SPECT images using an edge-preserving weighted regularization. 2017 IEEE 14th international symposium on biomedical imaging (ISBI 2017): IEEE; 2017. pp. 1074-77.
27. Gallivanone F, Stefano A, Grosso E, Canevari C, Gianolli L, Messa C, et al. PVE correction in PET-CT whole-body oncological studies from PVE-affected images. IEEE Trans Nucl Sci. 2011;58:736–47.
28. Quarantelli M, Berkouk K, Prinster A, Landeau B, Svarer C, Balkay L, et al. Integrated software for the analysis of brain PET/SPECT studies with partial-volume-effect correction. J Nucl Med. 2004;45:192–201.
29. Thomas BA, Erlandsson K, Reilhac A, Bousse A, Kazantsev D, Pedemonte S. A comparison of the options for brain partial volume correction using PET/MRI. 2012 IEEE Nuclear Science Symposium and Medical, Imaging et al. Conference Record (NSS/MIC): IEEE; 2012. pp. 2902-06.
30. Pretorius P, King M, Pan T, De Vries D, Glick S, Byrne C. Reducing the influence of the partial volume effect on SPECT activity quantitation with 3D modelling of spatial resolution in iterative reconstruction. Phys Med Biol. 1998;43:407.
31. Rahmim A, Qi J, Sossi V. Resolution modeling in PET imaging: theory, practice, benefits, and pitfalls. Med Phys. 2013;40:064301.
32. Meltzer CC, Frost J. Partial volume correction in emission-computed tomography: focus on alzheimer disease. Hallett M: Thatcher RW; 1994.
33. Thomas BA, Erlandsson K, Modat M, Thurfjell L, Vandenberghe R, Ourselin S, et al. The importance of appropriate partial volume correction for PET quantification in Alzheimer's disease. Eur J Nucl Med Mol Imaging. 2011;38:1104–19.
34. Erlandsson K, Buvat I, Pretorius PH, Thomas BA, Hutton BF. A review of partial volume correction techniques for emission tomography and their applications in neurology, cardiology and oncology. Phys Med Biol. 2012;57:R119-59.
35. Hoetjes NJ, van Velden FH, Hoekstra OS, Hoekstra CJ, Krak NC, Lammertsma AA, et al. Partial volume correction strategies for quantitative FDG PET in oncology. Eur J Nucl Med Mol Imaging. 2010;37:1679–87.
36. Bettinardi V, Castiglioni I, De Bernardi E, Gilardi M. PET quantification: strategies for partial volume correction. Clin Transl Imaging. 2014;2:199–218.
37. Kanetaka H, Matsuda H, Asada T, Ohnishi T, Yamashita F, Imabayashi E, et al. Effects of partial volume correction on discrimination between very early Alzheimer's dementia and controls using brain perfusion SPECT. Eur J Nucl Med Mol Imaging. 2004;31:975–80.
38. Arabi H, Asl ARK. Feasibility study of a new approach for reducing of partial volume averaging artifact in CT scanner. 2010 17th Iranian conference of biomedical engineering (ICBME): IEEE; 2010. pp. 1–4.
39. Zeraatkar N, Sajedi S, Farahani MH, Arabi H, Sarkar S, Ghafarian P, et al. Resolution-recovery-embedded image reconstruction for a high-resolution animal SPECT system. Phys Med. 2014;30:774–81.
40. Tang H, Brown J, Hasegawa B. Use of x-ray CT-defined regions of interest for the determination of SPECT recovery coefficients. IEEE Trans Nucl Sci. 1997;44:1594–9.
41. Da Silva AJ, Tang HR, Wong KH, Wu MC, Dae MW, Hasegawa BH. Absolute quantification of regional myocardial uptake of 99mTc-sestamibi with SPECT: experimental validation in a Porcine model. J Nucl Med. 2001;42:772–79.
42. Du Y, Tsui BM, Frey EC. Partial volume effect compensation for quantitative brain SPECT imaging. IEEE Trans Med Imaging. 2005;24:969–76.
43. Du Y, Tsui BM, Frey EC. Model-based compensation for quantitative ^{123}I brain SPECT imaging. Phys Med Biol. 2006;51:1269.
44. Boening G, Pretorius PH, King MA. Study of relative quantification of Tc-99 m with partial volume effect and spillover correction for SPECT oncology imaging. IEEE Trans Nucl Sci. 2006;53:1205–12.
45. Labbé C, Koepp M, Ashburner J, Spinks T, Richardson M, Duncan J, et al. Absolute PET quantification with correction for partial volume effects within cerebral structures. Quantitative functional brain imaging with positron emission tomography. Amsterdam: Elsevier; 1998.

46. Pain CD, Egan GF, Chen Z. Deep learning-based image reconstruction and post-processing methods in positron emission tomography for low-dose imaging and resolution enhancement. Eur J Nucl Med Mol Imaging. 2022;49:3098–118.
47. Jomaa H, Mabrouk R, Khlifa N. Post-reconstruction-based partial volume correction methods: a comprehensive review. Biomed Signal Process Control. 2018;46:131–44.
48. Alavi A, Werner TJ, Høilund-Carlsen PF, Zaidi H. Correction for partial volume effect is a must, not a luxury, to fully exploit the potential of quantitative PET imaging in clinical oncology. Mol Imaging Biol. 2018;20:1–3.
49. Tohka J. Partial volume effect modeling for segmentation and tissue classification of brain magnetic resonance images: a review. World J Radiol. 2014;6:855.
50. Marquis H, Willowson KP, Bailey DL. Partial volume effect in SPECT & PET imaging and impact on radionuclide dosimetry estimates. Asia Ocean J Nuclear Med Biology. 2023;11:44.
51. Marquis H, Schmidtlein CR, de Nijs R, Gabiña PM, Gustafsson J, Kayal G et al. MIRD pamphlet no. 32: a MIRD recovery coefficient model for resolution characterization and shape-specific partial-volume correction. J Nucl Med. 2025;66:457–65.
52. Müller-Gärtner HW, Links JM, Prince JL, Bryan RN, McVeigh E, Leal JP, et al. Measurement of radiotracer concentration in brain gray matter using positron emission tomography: MRI-based correction for partial volume effects. J Cereb Blood Flow Metab. 1992;12:571–83.
53. Teo B-K, Seo Y, Bacharach SL, Carrasquillo JA, Libutti SK, Shukla H, et al. Partial-volume correction in PET: validation of an iterative postreconstruction method with Phantom and patient data. J Nucl Med. 2007;48:802–10.
54. Moore SC, Southekal S, Park M-A, McQuaid SJ, Kijewski MF, Muller SP. Improved regional activity quantitation in nuclear medicine using a new approach to correct for tissue partial volume and spillover effects. IEEE Trans Med Imaging. 2011;31:405–16.
55. Southekal S, McQuaid SJ, Kijewski MF, Moore SC. Evaluation of a method for projection-based tissue-activity estimation within small volumes of interest. Phys Med Biol. 2012;57:685.
56. Cal-González J, Moore S, Park M, Herraiz J, Vaquero J, Desco M, et al. Improved quantification for local regions of interest in preclinical PET imaging. Phys Med Biol. 2015;60:7127.
57. Cal-Gonzalez J, Li X, Heber D, Rausch I, Moore SC, Schäfers K, et al. Partial volume correction for improved PET quantification in ^{18}F-NaF imaging of atherosclerotic plaques. J Nucl Cardiol. 2018;25:1742–56.
58. Panin VY, Kehren F, Michel C, Casey M. Fully 3-D PET reconstruction with system matrix derived from point source measurements. IEEE Trans Med Imaging. 2006;25:907–21.
59. Arabi H, AkhavanAllaf A, Sanaat A, Shiri I, Zaidi H. The promise of artificial intelligence and deep learning in PET and SPECT imaging. Phys Med. 2021;83:122–37.
60. Zaidi H, El Naqa I. Quantitative molecular positron emission tomography imaging using advanced deep learning techniques. Annu Rev Biomed Eng. 2021;23:249–76.
61. Balaji V, Song TA, Malekzadeh M, Heidari P, Dutta J. Artificial intelligence for PET and SPECT image enhancement. J Nucl Med. 2024;65:4–12.
62. Cal-Gonzalez J, Rausch I, Shiyam Sundar LK, Lassen ML, Muzik O, Moser E, et al. Hybrid imaging: instrumentation and data processing. Front Phys. 2018;6:47.
63. Vunckx K, Atre A, Baete K, Reilhac A, Deroose CM, Van Laere K, et al. Evaluation of three MRI-based anatomical priors for quantitative PET brain imaging. IEEE Trans Med Imaging. 2011;31:599–612.
64. Gutierrez D, Montandon M-L, Assal F, Allaoua M, Ratib O, Lövblad K-O, et al. Anatomically guided voxel-based partial volume effect correction in brain PET: impact of MRI segmentation. Comput Med Imaging Graph. 2012;36:610–9.
65. Tang J, Rahmim A. Anatomy assisted PET image reconstruction incorporating multi-resolution joint entropy. Phys Med Biol. 2014;60:31.
66. Dutta J, El Fakhri G, Zhu X, Li Q. PET point spread function modeling and image deblurring using a PET/MRI joint entropy prior. 2015 IEEE 12th international symposium on biomedical imaging (ISBI): IEEE; 2015. pp. 1423-26.
67. Belzunce MA, Mehranian A, Reader AJ. Enhancement of partial volume correction in MR-guided PET image reconstruction by using MRI voxel sizes. IEEE Trans Radiat Plasma Med Sci. 2018;3:315–26.
68. Bland J, Mehranian A, Belzunce MA, Ellis S, da Costa-Luis C, McGinnity CJ, et al. Intercomparison of MR-informed PET image reconstruction methods. Med Phys. 2019;46:5055–74.
69. Mehranian A, Belzunce MA, McGinnity CJ, Bustin A, Prieto C, Hammers A, et al. Multi-modal synergistic PET and MR reconstruction using mutually weighted quadratic priors. Magn Reson Med. 2019;81:2120–34.
70. Deidda D, Karakatsanis NA, Robson PM, Tsai Y-J, Efthimiou N, Thielemans K, et al. Hybrid PET-MR list-mode kernelized expectation maximization reconstruction. Inverse Probl. 2019;35:044001.
71. Chen KT, Salcedo S, Gong K, Chonde DB, Izquierdo-Garcia D, Drzezga A, et al. An efficient approach to perform MR-assisted PET data optimization in simultaneous PET/MR neuroimaging studies. J Nucl Med. 2019;60:272–8.
72. Mehranian A, Belzunce MA, Niccolini F, Politis M, Prieto C, Turkheimer F, et al. PET image reconstruction using multi-parametric anato-functional priors. Phys Med Biol. 2017;62:5975.
73. Zaidi H, Ruest T, Schoenahl F, Montandon M-L. Comparative evaluation of statistical brain MR image segmentation algorithms and their impact on partial volume effect correction in PET. Neuroimage. 2006;32:1591–607.
74. Bousse A, Pedemonte S, Thomas BA, Erlandsson K, Ourselin S, Arridge S, et al. Markov random field and Gaussian mixture for segmented MRI-based partial volume correction in PET. Phys Med Biol. 2012;57:6681.
75. Sattarivand M, Armstrong J, Szilagyi GM, Kusano M, Poon I, Caldwell C. Region-based partial volume correction techniques for PET imaging: sinogram implementation and robustness. Int J Mol Imaging. 2013. https://doi.org/10.1155/2013/435959.
76. Novosad P, Reader AJ. MR-guided dynamic PET reconstruction with the kernel method and spectral temporal basis functions. Phys Med Biol. 2016;61:4624.
77. Mehranian A, Belzunce MA, McGinnity CJ, Prieto C, Hammers A, Reader AJ. Multi-modal weighted quadratic priors for robust intensity independent synergistic PET-MR reconstruction. 2017 IEEE nuclear science symposium and medical imaging conference (NSS/MIC): IEEE; 2017. pp. 1–3.
78. Mehranian A, Zaidi H, Reader AJ. MR-guided joint reconstruction of activity and attenuation in brain PET-MR. Neuroimage. 2017;162:276–88.
79. Kang SK, Lee JS. Anatomy-guided PET reconstruction using l 1 bowsher prior. Phys Med Biol. 2021;66:095010.
80. Caldeira LL, da Silva N, Scheins JJ, Gaens ME, Shah NJ. Effects of regularisation priors and anatomical partial volume correction on dynamic PET data. IEEE Trans Nucl Sci. 2015;62:1725–31.
81. Turco A, Nuyts J, Gheysens O, Duchenne J, Voigt J-U, Claus P, et al. Lesion quantification and detection in myocardial 18F-FDG PET using edge-preserving priors and anatomical information from CT and MRI: A simulation study. EJNMMI Phys. 2016;3:1–32.

82. Sudarshan VP, Egan GF, Chen Z, Awate SP. Joint PET-MRI image reconstruction using a patch-based joint-dictionary prior. Med Image Anal. 2020;62:101669.
83. Hutchcroft W, Wang G, Chen KT, Catana C, Qi J. Anatomically-aided PET reconstruction using the kernel method. Phys Med Biol. 2016;61:6668.
84. Filipović M, Barat E, Dautremer T, Comtat C, Stute S. Pet reconstruction of the posterior image probability, including multimodal images. IEEE Trans Med Imaging. 2018;38:1643–54.
85. Turco A, Gheysens O, Duchenne J, Nuyts J, Rega F, Voigt J-U, et al. Partial volume and motion correction in cardiac PET: first results from an in vs ex vivo comparison using animal datasets. J Nucl Cardiol. 2019;26:2034–44.
86. Bauer CM, Cabral H, Greve D, Killiany R. Differentiating between normal aging, mild cognitive impairment, and alzheimer's disease with FDG-PET: effects of normalization region and partial volume correction method. J Alzheimers Dis Parkinsonism. 2013;3:113. https://doi.org/10.4172/2161-0460.1000113
87. Baker SL, Lockhart SN, Maass A, Jagust WJ. [P4–052]: Partial volume effects and medial temporal lobe tau quantitation with pet. Alzheimer's & Dementia. 2017;13:P1277-77.
88. Raptis E, Parkes L, Anton-Rodriguez J, Carter S, Herholz K, Matthews J. Investigation of the benefit of PVC in high resolution PET as a post and within reconstruction method for FDG brain data[preprint]. Research Square. 2020. https://doi.org/10.21203/rs.3.rs-44351/v1
89. Ibaraki M, Matsubara K, Shinohara Y, Shidahara M, Sato K, Yamamoto H, et al. Brain partial volume correction with point spreading function reconstruction in high-resolution digital PET: comparison with an MR-based method in FDG imaging. Ann Nucl Med. 2022;36:717–27.
90. Mandeville JB, Efthimiou N, Weigand-Whittier J, Hardy E, Knudsen GM, Jørgensen LM, et al. Partial volume correction of PET image data using geometric transfer matrices based on uniform B-splines. Phys Med Biol. 2024;69:055020.
91. Ashrafinia S, Karakatsanis N, Mohy-ud-Din H, Rahmim A. Towards continualized task-based resolution modeling in PET imaging. Med Imaging. 2014;2014(Physics of Medical Imaging: SPIE):625–30.
92. Cysouw MC, Kramer GM, Hoekstra OS, Frings V, de Langen AJ, Smit EF, et al. Accuracy and precision of partial-volume correction in oncological PET/CT studies. J Nucl Med. 2016;57:1642–49.
93. Ashrafinia S, Mohy-ud-Din H, Karakatsanis NA, Jha AK, Casey ME, Kadrmas DJ, et al. Generalized PSF modeling for optimized quantitation in PET imaging. Phys Med Biol. 2017;62:5149.
94. Ahn S, Asma E, Ross SG, Manjeshwar RM. Partial volume correction for penalized-likelihood image reconstruction in oncological PET applications. 2013 IEEE nuclear science symposium and medical imaging conference (2013 NSS/MIC): IEEE; 2013. pp. 1–4.
95. Meechai T, Tepmongkol S, Pluempitiwiriyawej C. Partial-volume effect correction in positron emission tomography brain scan image using super-resolution image reconstruction. Br J Radiol. 2015;88:20140119.
96. Bowen SL, Byars LG, Michel CJ, Chonde DB, Catana C. Influence of the partial volume correction method on ^{18}F-fluorodeoxyglucose brain kinetic modelling from dynamic PET images reconstructed with resolution model based OSEM. Phys Med Biol. 2013;58:7081.
97. Irace Z, Reilhac A, De Vigo BM, Batatia H, Costes N. PCA-based approach for inhomogeneous PSF estimation and partial volume correction in PET. 2016 IEEE nuclear science symposium, medical imaging conference and room-temperature semiconductor detector workshop (NSS/MIC/RTSD): IEEE; 2016. pp. 1–3.
98. Zhao J, Song Y, Liu Q, Chen S, Chen J-C. Optimization of the algorithm for the implementation of point spread function in the 3D-OSEM reconstruction algorithm based on the list-mode micro PET data. Electronics. 2023;12:1309.
99. Xu Z, Bagci U, Gao M, Mollura DJ. Highly precise partial volume correction for PET images: an iterative approach via shape consistency. 2015 IEEE 12th international symposium on biomedical imaging (ISBI): IEEE; 2015. pp. 1196-99.
100. Wu Z, Guo B, Huang B, Hao X, Wu P, Zhao B, et al. Phantom and clinical assessment of small pulmonary nodules using Q. clear reconstruction on a silicon-photomultiplier-based time-of-flight PET/CT system. Sci Rep. 2021;11(1):10328.
101. Turco A, Nuyts J, Duchenne J, Gheysens O, Voigt J-U, Claus P, et al. Analysis of partial volume correction on quantification and regional heterogeneity in cardiac PET. J Nucl Cardiol. 2020;27:62–70.
102. Lehnert W, Gregoire M-C, Reilhac A, Meikle SR. Characterisation of partial volume effect and region-based correction in small animal positron emission tomography (PET) of the rat brain. Neuroimage. 2012;60:2144–57.
103. Du Y, Madar I, Stumpf MJ, Rong X, Fung GS, Frey EC. Compensation for spill-in and spill-out partial volume effects in cardiac PET imaging. J Nucl Cardiol. 2013;20:84–98.
104. Wang H, Fei B. An MR image-guided, voxel-based partial volume correction method for PET images. Med Phys. 2012;39:179–94.
105. Yan J, Lim JC-S, Townsend DW. MRI-guided brain PET image filtering and partial volume correction. Phys Med Biol. 2015;60:961.
106. Gao Y, Zhu Y, Bilgel M, Ashrafinia S, Lu L, Rahmim A. Voxel-based partial volume correction of PET images via subtle MRI guided non-local means regularization. Phys Med. 2021;89:129–39.
107. Zhu Y, Bilgel M, Gao Y, Rousset OG, Resnick SM, Wong DF, et al. Deconvolution-based partial volume correction of PET images with parallel level set regularization. Phys Med Biol. 2021;66:145003.
108. Zhu Y, Gao Y, Rahmim A. Subtle MR guidance for partial volume correction of PET images: a comparison of techniques. 2019 IEEE nuclear science symposium and medical imaging conference (NSS/MIC): IEEE; 2019. pp. 1–3.
109. Gallivanone F, Canevari C, Mapelli P, Picchio M, Gianolli L, Gilardi MC, et al. Relationship between 18 F-FDG PET SUV with partial volume correction and histology in gastric and gastro-oesophageal cancer. Open Journal of Medical Imaging. 2012. https://doi.org/10.4236/ojmi.2012.23017
110. Gallivanone F, Canevari C, Sassi I, Zuber V, Marassi A, Gianolli L, et al. Partial volume corrected 18F-FDG PET mean standardized uptake value correlates with prognostic factors in breast cancer. Q J Nuclear Med Mol Imaging. 2014;58:424–39.
111. Picchio M, Kirienko M, Mapelli P, Dell'Oca I, Villa E, Gallivanone F, et al. Predictive value of pre-therapy ^{18} F-FDG PET/CT for the outcome of ^{18} F-FDG PET-guided radiotherapy in patients with head and neck cancer. Eur J Nucl Med Mol Imaging. 2014;41:21–31.
112. Gargouri S, Mouelhi A, Sayadi M, Labidi S, Mahersi M, Zayed S. Brief review of partial volume corrections in PET/CT for lung cancer assessment. 4th Int Conf Adv Technol Signal Image Process (ATSIP): IEEE. 2018;2018:1–6.
113. Taghvaei R, Zadeh MZ, Sirous R, Shamchi SP, Raynor WY, Seraj SM, et al. Pre-treatment partial-volume-corrected TLG is the best predictor of overall survival in patients with relapsing/refractory non-hodgkin lymphoma following radioimmunotherapy. Am J Nucl Med Mol Imaging. 2018;8:407.
114. Baun C, Falch K, Gerke O, Hansen J, Nguyen T, Alavi A, et al. Quantification of FDG-PET/CT with delayed imaging in patients

with newly diagnosed recurrent breast cancer. BMC Med Imaging. 2018;18:1–10.
115. Sattarivand M, Kusano M, Poon I, Caldwell C. Symmetric geometric transfer matrix partial volume correction for PET imaging: principle, validation and robustness. Phys Med Biol. 2012;57:7101.
116. McGinnity CJ, Shidahara M, Feldmann M, Keihaninejad S, Barros DAR, Gousias IS, et al. Quantification of opioid receptor availability following spontaneous epileptic seizures: correction of [11 C] diprenorphine PET data for the partial-volume effect. Neuroimage. 2013;79:72–80.
117. Evans E, Buonincontri G, Izquierdo D, Methner C, Hawkes RC, Ansorge RE, et al. Combining MRI with PET for partial volume correction improves image-derived input functions in mice. IEEE Trans Nucl Sci. 2015;62:628–33.
118. Funck T, Paquette C, Evans A, Thiel A. Surface-based partial-volume correction for high-resolution PET. Neuroimage. 2014;102:674–87.
119. Coello C, Willoch F, Selnes P, Gjerstad L, Fladby T, Skretting A. Correction of partial volume effect in ^{18}F-FDG PET brain studies using coregistered MR volumes: voxel based analysis of tracer uptake in the white matter. Neuroimage. 2013;72:183–92.
120. Kim E, Shidahara M, Tsoumpas C, McGinnity CJ, Kwon JS, Howes OD, et al. Partial volume correction using structural–functional synergistic resolution recovery: comparison with geometric transfer matrix method. J Cereb Blood Flow Metab. 2013;33:914–20.
121. Pandey AK, Sharma P, Pandey M, Aswathi K, Malhotra A, Kumar R. Spreadsheet program for estimating recovery coefficient to get partial volume corrected standardized uptake value in clinical positron emission tomography-computed tomography studies. Indian J Nucl Med. 2012;27:89.
122. Muellauer J, Willimayer R, Goertzen A, Wanek T, Langer O, Birkfellner W, et al. 18F, 11 C and 68Ga in small animal PET imaging. Nuklearmedizin. 2013;52(06):250–61.
123. Reeps C, Bundschuh RA, Pellisek J, Herz M, van Marwick S, Schwaiger M, et al. Quantitative assessment of glucose metabolism in the vessel wall of abdominal aortic aneurysms: correlation with histology and role of partial volume correction. Int J Cardiovasc Imaging. 2013;29:505–12.
124. Torigian DA, Dam V, Chen X, Saboury B, Udupa JK, Rashid A, et al. In vivo quantification of pulmonary inflammation in relation to emphysema severity via partial volume corrected (18) F-FDG-PET using computer-assisted analysis of diagnostic chest CT. Hell J Nucl Med. 2013;16:12–8.
125. Wang Y-W, Wu C-S, Chang C-H, Cheng K-S, Chang Y-K, Huang I-W, et al. Partial volume correction for equivocal retropharyngeal nodal metastases of nasopharyngeal carcinoma with fluorodeoxyglucose positron emission tomography–computed tomography. J Med Biol Eng. 2015;35:218–25.
126. Gallivanone F, Canevari C, Gianolli L, Salvatore C, Della Rosa P, Gilardi M, et al. A partial volume effect correction tailored for ^{18}F-FDG-PET oncological studies. BioMed Res Int. 2013. https://doi.org/10.1155/2013/780458.
127. Boivin G, Genoud V, Zaidi H. MRI-guided partial volume correction in brain PET imaging: comparison of five algorithms. Front Biomed Technol. 2014;1:73–81.
128. Giganti F, De Cobelli F, Canevari C, Orsenigo E, Gallivanone F, Esposito A, et al. Response to chemotherapy in gastric adenocarcinoma with diffusion-weighted MRI and 18F-FDG-PET/CT: correlation of apparent diffusion coefficient and partial volume corrected standardized uptake value with histological tumor regression grade. J Magn Reson Imaging. 2014;40:1147–57.
129. Grecchi E, O'Doherty J, Veronese M, Tsoumpas C, Cook GJ, Turkheimer FE. Multimodal partial-volume correction: application to ^{18}F-fluoride PET/CT bone metastases studies. J Nucl Med. 2015;56:1408–14.
130. Ortega C, Schaefferkoetter J, Veit-Haibach P, Anconina R, Berlin A, Perlis N, et al. 18F-DCFPyL PET/CT in patients with subclinical recurrence of prostate cancer: effect of lesion size, smoothing filter, and partial-volume correction on PROMISE criteria. J Nucl Med. 2020;61:1615–20.
131. Lue K-H, Lin H-H, Kao C-HK, Hsieh H-J, Liu S-H, Chuang K-S. A simple algorithm for subregional striatal uptake analysis with partial volume correction in dopaminergic PET imaging. Ann Nucl Med. 2014;28:33–41.
132. Li X, Zhang M, Huang P, Liu W, Huang Q. An investigation into the impact of partial volume correction on detection rate of epilepsy using 18F-FDG PET. BIBE 2019; The third international conference on biological information and biomedical engineering: VDE; 2019. pp. 1–5.
133. Raptis E, Parkes LM, Anton-Rodriguez JM, Carter SF, Herholz K, Matthews JC. Evaluation of the Benefit of Partial Volume Correction for High Resolution PET Scanners. 2019 IEEE nuclear science symposium and medical imaging conference (NSS/MIC): IEEE; 2019. pp. 1–3.
134. Greve DN, Svarer C, Fisher PM, Feng L, Hansen AE, Baare W, et al. Cortical surface-based analysis reduces bias and variance in kinetic modeling of brain PET data. Neuroimage. 2014;92:225–36.
135. Jones G, O'Keefe G, Veljanovski R, Williams R, Masters CL, Rowe CC, et al. IC-P-198: ASSESSING THE ACCURACY OF A CT-BASED APPROACH TO THE PARTIAL VOLUME CORRECTION OF FLUTEMETAMOL-PET IMAGES. Alzheimer's &. Dementia. 2014;10:P110–10.
136. Bural G, Torigian D, Basu S, Houseni M, Zhuge Y, Rubello D, et al. Partial volume correction and image segmentation for accurate measurement of standardized uptake value of grey matter in the brain. Nucl Med Commun. 2015;36:1249–52.
137. Salavati A, Borofsky S, Boon-Keng TK, Houshmand S, Khiewvan B, Saboury B, et al. Application of partial volume effect correction and 4D PET in the quantification of FDG avid lung lesions. Mol Imaging Biol. 2015;17:140–8.
138. Niesporek SC, Hoffmann SH, Berger MC, Benkhedah N, Kujawa A, Bachert P, et al. Partial volume correction for in vivo 23Na-MRI data of the human brain. Neuroimage. 2015;112:353–63.
139. Schwarz CG, Gunter JL, Lowe VJ, Weigand S, Vemuri P, Senjem ML, et al. A comparison of partial volume correction techniques for measuring change in serial amyloid PET SUVR. J Alzheimers Dis. 2019;67:181–95.
140. Rausch I, Beitzke D, Li X, Pfaff S, Rasul S, Haug AR, et al. Accuracy of PET quantification in [68Ga] Ga-pentixafor PET/MR imaging of carotid plaques. J Nucl Cardiol. 2022;29:492–502.
141. Cal-González J, Tsoumpas C, Lassen M, Rasul S, Koller L, Hacker M, et al. Impact of motion compensation and partial volume correction for ^{18}F-NaF PET/CT imaging of coronary plaque. Phys Med Biol. 2017;63:015005.
142. Turco A, Duchenne J, Gheysens O, Nuyts J, Voigt J, Claus P, Partial volume correction of doubly-gated cardiac datasets using anatomical and edge-preserving priors., Conference et al. (NSS/MIC): IEEE; 2015. pp. 1–4.
143. Greve DN, Salat DH, Bowen SL, Izquierdo-Garcia D, Schultz AP, Catana C, et al. Different partial volume correction methods lead to different conclusions: an 18F-FDG-PET study of aging. Neuroimage. 2016;132:334–43.
144. Thomas BA, Cuplov V, Bousse A, Mendes A, Thielemans K, Hutton BF, et al. PETPVC: a toolbox for performing partial volume correction techniques in positron emission tomography. Phys Med Biol. 2016;61:7975.

145. Sasaki K, Maikusa N, Imabayashi E, Yuasa T, Matsuda H. The feasibility of 11 C-PIB-PET/CT for amyloid plaque burden: validation of the effectiveness of CT-based partial volume correction. Brain Behav. 2016;6:e00532.
146. Yang J, Hu C, Guo N, Dutta J, Vaina LM, Johnson KA, et al. Partial volume correction for PET quantification and its impact on brain network in Alzheimer's disease. Sci Rep. 2017;7:13035.
147. Shigemoto Y, Sone D, Imabayashi E, Maikusa N, Okamura N, Furumoto S, et al. Dissociation of tau deposits and brain atrophy in early Alzheimer's disease: a combined positron emission tomography/magnetic resonance imaging study. Front Aging Neurosci. 2018;10:223.
148. Lu Y, Toyonaga T, Naganawa M, Gallezot J-D, Chen M-K, Mecca AP, et al. Partial volume correction analysis for 11 C-UCB-J PET studies of Alzheimer's disease. Neuroimage. 2021;238:118248.
149. Su Y, Blazey TM, Snyder AZ, Raichle ME, Marcus DS, Ances BM, et al. Partial volume correction in quantitative amyloid imaging. Neuroimage. 2015;107:55–64.
150. Schwarz CG, Senjem ML, Gunter JL, Tosakulwong N, Weigand SD, Kemp BJ, et al. Optimizing PiB-PET SUVR change-over-time measurement by a large-scale analysis of longitudinal reliability, plausibility, separability, and correlation with MMSE. Neuroimage. 2017;144:113–27.
151. Matsubara K, Ibaraki M, Shidahara M, Kinoshita T, Initiative ADN. Iterative framework for image registration and partial volume correction in brain positron emission tomography. Radiol Phys Technol. 2020;13(4):348–57.
152. Minhas DS, Price JC, Laymon CM, Becker CR, Klunk WE, Tudorascu DL, et al. Impact of partial volume correction on the regional correspondence between in vivo [C-11] PiB PET and postmortem measures of Aβ load. NeuroImage: Clinical. 2018;19:182–9.
153. Sur C, Adamczuk K, Scott D, Kost J, Sampat M, Buckley C, et al. Evaluation of 18F-flutemetamol amyloid PET image analysis parameters on the effect of verubecestat on brain amlyoid load in Alzheimer's disease. Mol Imaging Biol. 2022;24:862–73.
154. Gao Y, Zhang H, Zhu Y, Bilgel M, Rousset O, Resnick S et al. Voxel-based partial volume correction of amyloid PET images incorporating non-local means regularization. 2018 IEEE nuclear science symposium and medical imaging conference proceedings (NSS/MIC): IEEE; 2018; pp. 1–4.
155. Costoya-Sánchez A, Moscoso A, Sobrino T, Ruibal Á, Grothe MJ, Schöll M, et al. Partial volume correction in longitudinal Tau PET studies-is it really needed? NeuroImage. 2024;289:120537. https://doi.org/10.1016/j.neuroimage.2024.120537
156. Malpas CB, Saling MM, Velakoulis D, Desmond P, Hicks RJ, O'Brien TJ. Longitudinal partial volume correction in 2-[18F]-fluoro-2-deoxy-D-glucose positron emission tomography studies of Alzheimer disease. J Comput Assist Tomogr. 2015;39:559.
157. Matsubara K, Ibaraki M, Shimada H, Ikoma Y, Suhara T, Kinoshita T, et al. Impact of spillover from white matter by partial volume effect on quantification of amyloid deposition with [^{11}C] PiB PET. Neuroimage. 2016;143:316–24.
158. Eldib M, Oesingmann N, Faul DD, Kostakoglu L, Knešaurek K, Fayad ZA. Optimization of yttrium-90 PET for simultaneous PET/MR imaging: a phantom study. Med Phys. 2016;43:4768–74.
159. Kaida H, Azuma K, Kawahara A, Takamori S, Akiba J, Fujimoto K, et al. Prognostic value of dual-point fluorine-18 Fluorodeoxyglucose PET imaging, partial volume correction and glucose transporter-1 expression in resected nonsmall cell lung cancer patients. Nucl Med Commun. 2020;41:48–57.
160. Lee SH, Ha S, An HJ, Lee JS, Han W, Im S-A, et al. Association between partial-volume corrected SUV max and oncotype DX recurrence score in early-stage, ER-positive/HER2-negative invasive breast cancer. Eur J Nucl Med Mol Imaging. 2016;43:1574–84.
161. Grecchi E, Veronese M, Bodini B, García-Lorenzo D, Battaglini M, Stankoff B, et al. Multimodal partial volume correction: application to [11 C] PIB PET/MRI myelin imaging in multiple sclerosis. J Cereb Blood Flow Metab. 2017;37:3803–17.
162. Shidahara M, Thomas BA, Okamura N, Ibaraki M, Matsubara K, Oyama S, et al. A comparison of five partial volume correction methods for Tau and amyloid PET imaging with [18 F] THK5351 and [11 C] PIB. Ann Nucl Med. 2017;31:563–9.
163. Oyama S, Hosoi A, Ibaraki M, McGinnity CJ, Matsubara K, Watanuki S, et al. Error propagation analysis of seven partial volume correction algorithms for [18 F] THK-5351 brain PET imaging. EJNMMI Phys. 2020;7:1–15.
164. Sari H, Erlandsson K, Law I, Larsson HB, Ourselin S, Arridge S, et al. Estimation of an image derived input function with MR-defined carotid arteries in FDG-PET human studies using a novel partial volume correction method. J Cereb Blood Flow Metab. 2017;37:1398–409.
165. Baker SL, Maass A, Jagust WJ. Considerations and code for partial volume correcting [18F]-AV-1451 tau PET data. Data Brief. 2017;15:648–57.
166. Fazio P, Schain M, Mrzljak L, Amini N, Nag S, Al-Tawil N, et al. Patterns of age related changes for phosphodiesterase type-10A in comparison with dopamine D2/3 receptors and sub-cortical volumes in the human basal ganglia: a PET study with 18F-MNI-659 and 11 C-raclopride with correction for partial volume effect. Neuroimage. 2017;152:330–9.
167. Wolters EE, Golla SS, Timmers T, Ossenkoppele R, van der Weijden CW, Scheltens P, et al. A novel partial volume correction method for accurate quantification of [18 F] flortaucipir in the hippocampus. EJNMMI Res. 2018;8:1–5.
168. López-González FJ, Costoya-Sánchez A, Paredes-Pacheco J, Moscoso A, Silva-Rodríguez J, Aguiar P. Impact of spill-in counts from off-target regions on [18F] flortaucipir PET quantification. Neuroimage. 2022;259:119396.
169. Sanabria Bohórquez SM, Baker S, Manser PT, Tonietto M, Galli C, Wildsmith KR, et al. Evaluation of partial volume correction and analysis of longitudinal [18F] GTP1 tau PET imaging in Alzheimer's disease using linear mixed-effects models. Front Neuroimaging. 2024;3:1355402.
170. van Aalst J, Devrome M, Van Weehaeghe D, Rezaei A, Radwan A, Schramm G, et al. Regional glucose metabolic decreases with ageing are associated with microstructural white matter changes: a simultaneous PET/MR study. Eur J Nucl Med Mol Imaging. 2022;49:664–80.
171. Funck T, Larcher K, Toussaint P-J, Evans AC, Thiel A. APPIAN: automated pipeline for PET image analysis. Front Neuroinform. 2018;12:64.
172. Smith CT, Crawford JL, Dang LC, Seaman KL, San Juan MD, Vijay A, et al. Partial-volume correction increases estimated dopamine D2-like receptor binding potential and reduces adult age differences. J Cereb Blood Flow Metab. 2019;39:822–33.
173. Ferraro PM, Campi C, Miceli A, Rolla-Bigliani C, Bauckneht M, Gualco L, et al. 18F-FDG-PET correlates of aging and disease course in ALS as revealed by distinct PVC approaches. Eur J Radiol Open. 2022;9:100394.
174. Scott MR, Edwards NC, Properzi MJ, Jacobs HI, Price JC, Lois C, et al. Contribution of extracerebral tracer retention and partial volume effects to sex differences in Flortaucipir-PET signal. J Cereb Blood Flow Metab. 2024;44:131–41.
175. Paranjpe MD, Chen X, Liu M, Paranjpe I, Leal JP, Wang R, et al. The effect of ApoE ε4 on longitudinal brain region-specific glucose metabolism in patients with mild cognitive impairment: a FDG-PET study. NeuroImage: Clinical. 2019;22:101795.
176. Hellem MN, Vinther-Jensen T, Anderberg L, Budtz-Jørgensen E, Hjermind LE, Larsen VA, et al. Hybrid 2-[18F] FDG PET/MRI in premanifest Huntington's disease gene-expansion

carriers: the significance of partial volume correction. PLoS ONE. 2021;16:e0252683.
177. Cysouw MCF, Golla SVS, Frings V, Smit EF, Hoekstra OS, Kramer GM, et al. Partial-volume correction in dynamic PET-CT: effect on tumor kinetic parameter estimation and validation of simplified metrics. EJNMMI Res. 2019;9:12.
178. Teipel SJ, Dyrba M, Vergallo A, Lista S, Habert MO, Potier M-C, et al. Partial volume correction increases the sensitivity of ^{18}F-florbetapir-positron emission tomography for the detection of early stage amyloidosis. Front Aging Neurosci. 2021;13:748198.
179. Laymon CM, Minhas DS, Royse SK, Aizenstein HJ, Cohen AD, Tudorascu DL, et al. Characterization of point-spread function specification error on geometric transfer matrix partial volume correction in [11 C] PiB amyloid imaging. EJNMMI Phys. 2021;8:1–16.
180. Ayubcha C, Raynor WY, Borja AJ, Seraj SM, Rojulpote C, Werner TJ, et al. Magnetic resonance imaging-based partial volume-corrected ^{18}F-sodium fluoride positron emission tomography in the femoral neck. Nucl Med Commun. 2021;42:416–20.
181. Zadeh MZ, Asadollahi S, Kaghazchi F, Raynor WY, Seraj SM, Werner TJ, et al. Prognostic significance of conventional and volumetric PET parameters with and without partial volume correction in the assessment of head and neck squamous cell carcinoma. Nucl Med Commun. 2022;43:800–6.
182. Guo B, Huang B, Li X, Zhao J, Li Y, Li S et al. Effect of different β values combined with partial volume effect correction on the semi-quantitative accuracy and image quality of 68Ga-PSMA PET/CT. Chin J Nuclear Med Mol Imaging. 2022;42(6):401–5.
183. Mertens N, Michiels L, Vanderlinden G, Vandenbulcke M, Lemmens R, Van Laere K, et al. Impact of meningeal uptake and partial volume correction techniques on [18F] MK-6240 binding in amci patients and healthy controls. J Cereb Blood Flow Metab. 2022;42:1236–46.
184. Kafkaletos A, Mix M, Sachpazidis I, Carles M, Rühle A, Ruf J, et al. The significance of partial volume effect on the estimation of hypoxic tumour volume with [18F] FMISO PET/CT. EJNMMI Phys. 2024;11:43.
185. Kafkaletos A, Sachpazidis I, Mix M, Carles M, Schäfer H, Rühle A, et al. Implications of the partial volume effect correction on the spatial quantification of hypoxia based on [18F] FMISO PET/CT data. Phys Med. 2024;128:104853.
186. Danesh K, Azimi M, Sharifian P, Karimian A, Arabi H, Zaidi H. Anatomical Brain Segmentation from CT images in brain PET/CT imaging for the purpose of partial volume correction in PET imaging. 2024 IEEE nuclear science symposium (NSS), Medical imaging conference (MIC) and room temperature semiconductor detector conference (RTSD): IEEE; 2024. pp. 1–2.
187. Dumouchel T, Thorn S, Kordos M, DaSilva J, Beanlands RS, Robert Ad. A three-dimensional model-based partial volume correction strategy for gated cardiac mouse PET imaging. Phys Med Biol. 2012;57:4309.
188. Hofheinz F, Langner J, Petr J, Beuthien-Baumann B, Oehme L, Steinbach J, et al. A method for model-free partial volume correction in oncological PET. EJNMMI Res. 2012;2:1–12.
189. Hatt M, Le Pogam A, Visvikis D, Pradier O, Le Rest CC. Impact of partial-volume effect correction on the predictive and prognostic value of baseline 18F-FDG PET images in esophageal cancer. J Nucl Med. 2012;53:12–20.
190. Hatt M, Tixier F, Le Rest CC, Visvikis D. SU-D-500-04: impact of delineation and partial volume effects correction on PET uptake heterogeneity quantification through textural features analysis for therapy response in oncology. Med Phys. 2013;40:106–06.
191. Hatt M, Van Stiphout R, Le Pogam A, Lammering G, Visvikis D, Lambin P. Early prediction of pathological response in locally advanced rectal cancer based on sequential ^{18}F-FDG PET. Acta Oncol. 2013;52:619–26.
192. Hatt M, Tixier F, Le Cheze C, Pradier O, Visvikis D. Robustness of intratumour 18 F-FDG PET uptake heterogeneity quantification for therapy response prediction in oesophageal carcinoma. Eur J Nucl Med Mol Imaging. 2013;40:1662–71.
193. Stefano S, Gallivanone A, Messa F, Gilardi C, Gastiglioni M. Metabolic impact of partial volume correction of [18F] FDG PET-CT oncological studies on the assessment of tumor response to treatment. Q J of Nuclear Med Mol Imaging: Official Publication of Italian Association of Nuclear Med (AIMN)[and] Int Association of Radiopharmacology (IAR) [and] Sect of Soc of. 2014;58:413–23.
194. Mikasa S, Akamatsu G, Taniguchi T, Kidera D, Kihara K, Matsuoka K et al. Standardization of dual time point [18F] 2-Deoxy-2-fluoro-D-glucose-positron emission tomography performed with different positron emission tomography scanners using partial volume correction. Res Rep Nuclear Med. 2015;5:1–7. https://doi.org/10.2147/RRNM.S73413
195. Golla SS, Lubberink M, van Berckel BN, Lammertsma AA, Boellaard R. Partial volume correction of brain PET studies using iterative Deconvolution in combination with HYPR denoising. EJNMMI Res. 2017;7:1–12.
196. Akerele M, Wadhwa P, Vandenberghe S, Tsoumpas C. Comparison of partial volume correction techniques for lesions near high activity regions. 2017 IEEE nuclear science symposium and medical imaging conference (NSS/MIC): IEEE; 2017. pp. 1–7.
197. Arakawa R, Stenkrona P, Takano A, Nag S, Maior RS, Halldin C. Test-retest reproducibility of [11 C]-l-deprenyl-D 2 binding to MAO-B in the human brain. EJNMMI Res. 2017;7:1–7.
198. Mackova K, Ptacek J, Ters J, Dudasova K, Janca R. Effective Image Resolution for Partial Volume Correction in FDG-PET Brain Imaging: A Proof of Concept. 2025 IEEE medical measurements & applications (MeMeA): IEEE; 2025. pp. 1–6
199. Hammersen N, Jentzen W, Stawitzki F, Herrmann K, Kersting D, Costa PF, et al. PET quantification performance of the oversize-volume-of-interest approach in the context of tumour dosimetry in radionuclide therapy planning. Phys Med Biol. 2024;69:165007.
200. Azimi MS, Cheraghi M, MahdiMaleki F, MahdiMaleki F, Sanaat A, Høilund-Carlsen PF, et al. Toward standardization: assessing the reproducibility of radiomics features in partial volume-corrected brain PET images. Neuroimage. 2025. https://doi.org/10.1016/j.neuroimage.2025.121398.
201. Xu Z, Gao M, Papadakis GZ, Luna B, Jain S, Mollura DJ, et al. Joint solution for PET image segmentation, denoising, and partial volume correction. Med Image Anal. 2018;46:229–43.
202. Song T-A, Chowdhury SR, Kim K, Gong K, El Fakhri G, Li Q, Super-resolution PET using a very deep convolutional neural network. 2018 IEEE nuclear science symposium and medical, imaging et al. Conference proceedings (NSS/MIC): IEEE; 2018. pp. 1–2.
203. Zhao Q, Liu M, Zhou Y. Quantitative ^{18}F-AV1451 brain tau PET imaging in cognitively normal older adults, mild cognitive impairment, and Alzheimer's disease patients. Front Neurol. 2019;10:425111.
204. Corda-D'Incan G, Schnabel JA, Reader AJ. Syn-net for synergistic deep-learned pet-mr reconstruction. 2020 IEEE Nuclear Science Symposium and Medical Imaging Conference (NSS/MIC): IEEE; 2020. pp. 1–5.
205. Matsubara K, Ibaraki M, Kinoshita T, Initiative AsDN. Deeppvc: prediction of a partial volume-corrected map for brain positron emission tomography studies via a deep convolutional neural network. EJNMMI Phys. 2022;9:50.
206. Corda-D'Incan G, Schnabel JA, Reader AJ. Anato-functional adaptive regularisation for deep learned MR-guided PET reconstruction. 2022 IEEE nuclear science symposium and medical imaging conference (NSS/MIC): IEEE; 2022. pp. 1–4.

207. Campanioni S, González-Nóvoa JA, Busto L, Agís-Balboa RC. Data-driven phenotyping of Alzheimer's disease under epigenetic conditions using partial volume correction of PET studies and manifold learning. Biomedicines. 2023;11:273.
208. Liu Z, Zhu Y, Fu R, Gao Y. Partial volume correction for PET imaging based on deep image priorpartial volume correction for PET imaging based on deep image prior. 2023 IEEE nuclear science symposium, medical imaging conference and international symposium on room-temperature semiconductor detectors (NSS MIC RTSD): IEEE; 2023. pp. 1–1.
209. Marsh IR, Li C, Grudzinski J, Jeffery J, Longhurst C, Adam DP, et al. Targeting of head and neck cancer by radioiodinated CLR1404 in murine xenograft tumor models with partial volume corrected theranostic dosimetry. Cancer Biother Radiopharm. 2023;38:458–67.
210. Farag A, Huang J, Kohan A, Mirshahvalad SA, Dias AB, Fenchel M, et al. Evaluation of MR anatomically-guided PET reconstruction using a convolutional neural network in PSMA patients. Phys Med Biol. 2023;68:185014.
211. Corda-D'Incan G, Schnabel JA, Hammers A, Reader AJ. Single-modality supervised joint PET-MR image reconstruction. IEEE Trans Radiat Plasma Med Sci.2023;7(7):742–54. https://doi.org/10.1109/TRPMS.2023.3283786
212. Shah J, Che Y, Sohankar J, Luo J, Li B, Su Y, et al. Enhancing amyloid PET quantification: MRI-guided super-resolution using latent diffusion models. Life. 2024;14:1580.
213. Jomaa H, Mabrouk R, Khlifa N. Partial volume effect correction in PET image using iterative deconvolution and shearlet transform. 2018 4th international conference on advanced technologies for signal and image processing (ATSIP): IEEE; 2018. pp. 1–6.
214. Sanaat A, Shooli H, Böhringer AS, Sadeghi M, Shiri I, Salimi Y, et al. A cycle-consistent adversarial network for brain PET partial volume correction without prior anatomical information. Eur J Nucl Med Mol Imaging. 2023;50:1881–96.
215. Azimi M-S, Kamali-Asl A, Ay M-R, Zeraatkar N, Hosseini M-S, Sanaat A, et al. Deep learning-based partial volume correction in standard and low-dose positron emission tomography-computed tomography imaging. Quant Imaging Med Surg. 2024;14(3):2146. https://doi.org/10.21037/qims-23-871
216. Azimi M, Kamali-Asl A, Ay M-R, Zeraatkar N, Hosseini M-S, Sanaat A, et al. Attention-based deep neural network for partial volume correction in brain 18F-FDG PET imaging. Phys Med. 2024;119:103315.
217. Lin Y-N, Huang S-Y, Chung M-C, Tsai C-H, Wang H-W, Gong E, et al. MRI-styled PET: a dual modality fusion approach to PET partial volume correction. IEEE Trans Radiat Plasma Med Sci. 2025. https://doi.org/10.1109/TRPMS.2025.3549617.
218. Erlandsson K, Hutton BF. Partial volume correction in SPECT using anatomical information and iterative FBP. Tsinghua Sci Technol. 2010;15:50–5.
219. Erlandsson K, Thomas B, Dickson J, Hutton BF. Partial volume correction in SPECT reconstruction with OSEM. Nucl Instrum Methods Phys Res A. 2011;648:S85–8.
220. Chan C, Liu H, Grobshtein Y, Stacy MR, Sinusas AJ, Liu C. Simultaneous partial volume correction and noise regularization for cardiac SPECT/CT. 2013 IEEE nuclear science symposium and medical imaging conference (2013 NSS/MIC): IEEE; 2013. pp. 1–6.
221. Liu H, Chan C, Grobshtein Y, Ma T, Liu Y, Wang S, et al. Anatomical-based partial volume correction for low-dose dedicated cardiac SPECT/CT. Phys Med Biol. 2015;60:6751.
222. Chan C, Liu H, Grobshtein Y, Stacy MR, Sinusas AJ, Liu C. Noise suppressed partial volume correction for cardiac SPECT/CT. Med Phys. 2016;43:5225–39.
223. Kangasmaa TS, Constable C, Sohlberg AO. Quantitative bone SPECT/CT reconstruction utilizing anatomical information. EJNMMI Phys. 2021;8:1–14.
224. Marquis H, Deidda D, Gillman A, Willowson K, Gholami Y, Hioki T, et al. Theranostic SPECT reconstruction for improved resolution: application to radionuclide therapy dosimetry. EJNMMI Phys. 2021;8:1–17.
225. Vuohijoki HE, Constable CJ, Sohlberg AO. Anatomically guided reconstruction improves lesion quantitation and detectability in bone SPECT/CT. Nucl Med Commun. 2023;44:330–7.
226. Morphis M, Van Staden J, du Raan H. O32. technetium-99m and gold-198 activity quantification using SPECT/CT monte carlo simulations. Phys Med. 2016;32:151.
227. Leube J, Claeys W, Gustafsson J, Salas-Ramirez M, Lassmann M, Koole M, et al. Position dependence of recovery coefficients in 177Lu-SPECT/CT reconstructions–phantom simulations and measurements. EJNMMI Phys. 2024;11:52.
228. De Schepper S, Gnanasegaran G, De Vos W, Van de Casteele E, Dickson JC, Van den Wyngaert T. From SPECT/CT towards absolute quantification?-the case of unilateral condylar hyperplasia of the mandible. EJNMMI Phys. 2024;11:74.
229. Liu Q, Mohy-ud-Din H, Boutagy NE, Jiang M, Ren S, Stendahl JC, et al. Fully automatic multi-atlas segmentation of CTA for partial volume correction in cardiac SPECT/CT. Phys Med Biol. 2017;62:3944.
230. Wu J, Liu H, Hashemi Zonouz T, Sandoval VM, Mohy-ud-Din H, Lampert RJ, et al. A blind deconvolution method incorporated with anatomical-based filtering for partial volume correction: validations with 123I-mIBG cardiac SPECT/CT. Med Phys. 2017;44:6435–46.
231. Ito Y, Fujita N, Hara K, Tada T, Abe S, Katsuno M, et al. New semi-quantification approach for dopamine transporter scan. Quantification of accumulation by examining the approximate image; 2020.
232. Ren C, Ren J, Tian Z, Du Y, Hao Z, Zhang Z, et al. Assessment of cardiac amyloidosis with 99m Tc-pyrophosphate (PYP) quantitative SPECT. EJNMMI Phys. 2021;8:1–16.
233. Ito Y, Fujita N, Hara K, Tada T, Abe S, Katsuno M, et al. Novel approach to semi-quantification of tracer accumulation in dopamine transporter scan. J Appl Clin Med Phys. 2022;23:e13626.
234. Mohy-ud-Din H, Boutagy NE, Stendahl JC, Zhuang ZW, Sinusas AJ, Liu C. Quantification of intramyocardial blood volume with 99mTc-RBC SPECT-CT imaging: a preclinical study. J Nucl Cardiol. 2018;25:2096–111.
235. Yin T-K, Lee B-F, Yang YK, Chiu N-T. Differences of various region-of-interest methods for measuring dopamine transporter availability using-TRODAT-1 SPECT. The scientific world journal. 2014;2014.
236. Tran-Gia J, Salas-Ramirez M, Lassmann M. What you see is not what you get: on the accuracy of voxel-based dosimetry in molecular radiotherapy. J Nucl Med. 2020;61(8):1178–86.
237. Ramonaheng K, van Staden JA, du Raan H. The effect of calibration factors and recovery coefficients on 177 Lu SPECT activity quantification accuracy: a Monte Carlo study. EJNMMI Phys. 2021;8:1–23.
238. Grings A, Jobic C, Kuwert T, Ritt P. The magnitude of the partial volume effect in SPECT imaging of the kidneys: a phantom study. EJNMMI Phys. 2022;9:18.
239. Jalilifar M, Sadeghi M, Emami-Ardekani A, Geravand K, Geramifar P. Quantifying partial volume effect in SPECT and planar imaging: optimizing region of interest for activity concentration estimation in different sphere sizes. Nucl Med Commun. 2024;45(6):487–98. https://doi.org/10.1097/MNM.0000000000001835

240. Azimi M-S, Maroufpour S, Hosseini M-S, Zahed A, Alhashim M, Dadgar H et al. Effect of partial volume correction on kernel-based dosimetry for Lu-177-PSMA therapy with SPECT/CT Imaging. 2024 IEEE nuclear science symposium (NSS), medical imaging conference (MIC) and room temperature semiconductor detector conference (RTSD): IEEE; 2024. pp. 1–2.
241. Rumiantcev M, Resch S, Liubchenko G, Sheikh G, Zacherl M, Werner RA, et al. Feasibility of automated image-based red bone marrow dosimetry for [177Lu] Lu-PSMA radiopharmaceutical therapy of metastatic castration-resistant prostate cancer. Cancers. 2025;17:2313.
242. Adam DP, Grudzinski JJ, Bormett I, Cox BL, Marsh IR, Bradshaw TJ, et al. Validation of monte carlo ^{131}I radiopharmaceutical dosimetry workflow using a 3D-printed anthropomorphic head and neck phantom. Med Phys. 2022;49:5491–503.
243. Yousefi H, Shi L, Soufer A, Tsatkin V, Bruni W, Avendano R, et al. Quantification of intramyocardial blood volume using 99mTc-RBC SPECT/CT: a pilot human study. J Nucl Cardiol. 2023;30:292–7.
244. Gillen R, Erlandsson K, Denis-Bacelar AM, Thielemans K, Hutton BF, McQuaid SJ. Towards accurate partial volume correction in 99mTc oncology SPECT: perturbation for case-specific resolution estimation. EJNMMI Phys. 2022;9:59.
245. Xie H, Liu Z, Shi L, Greco K, Chen X, Zhou B et al. Segmentation-free PVC for cardiac SPECT using a densely-connected multi-dimensional dynamic network. IEEE Trans Med Imaging. 2022;42(5):1325–36. https://doi.org/10.1109/TMI.2022.3226604
246. Leube J, Gustafsson J, Lassmann M, Salas-Ramirez M, Tran-Gia J. A Deep-learning–based partial-volume correction method for quantitative ^{177}Lu SPECT/CT imaging. J Nuclear Med. 2024:jnumed.123.266889.
247. Wang B, Wang H, Huang W, Hung G-U, Hu Z, Mok G. Evaluation of Deep Learning-based partial volume correction on clinical 99mTc-TRODAT-1 SPECT using a no-gold standard technique. 2024 IEEE nuclear science symposium (NSS), medical imaging conference (MIC) and room temperature semiconductor detector conference (RTSD): IEEE; 2024. pp. 1–2.
248. Wang H, Wang B, Huang W, Liu Y, Du Y, Hung G-U et al. Deep-learning-based partial volume correction in 99mTc-TRODAT-1 SPECT for Parkinson's disease: a preliminary study on clinical translation. IEEE J Biomedical Health Inf. 2025.
249. Cysouw MCF, Kramer GM, Schoonmade LJ, Boellaard R, de Vet HCW, Hoekstra OS. Impact of partial-volume correction in oncological PET studies: a systematic review and meta-analysis. Eur J Nucl Med Mol Imaging. 2017;44:2105–16.
250. Erlandsson K, Dickson J, Arridge S, Atkinson D, Ourselin S, Hutton BF. Mr imaging-guided partial volume correction of PET data in PET/MR imaging. PET Clin. 2016;11:161–77.
251. Zhu Y, Zhu X. MRI-driven PET image optimization for neurological applications. Front Neurosci. 2019;13:433123.
252. deKemp RA, Wells RG, Beanlands RS. Lesion contrast recovery for partial-volume averaging: quantitative correction or qualitative enhancement? Springer; 2018. pp. 1757–59.
253. Aide N, Lasnon C, Veit-Haibach P, Sera T, Sattler B, Boellaard R. EANM/EARL harmonization strategies in PET quantification: from daily practice to multicentre oncological studies. Eur J Nucl Med Mol Imaging. 2017;44:17–31.
254. Gear JI, Cox MG, Gustafsson J, Gleisner KS, Murray I, Glatting G, et al. EANM practical guidance on uncertainty analysis for molecular radiotherapy absorbed dose calculations. Eur J Nucl Med Mol Imaging. 2018;45:2456–74.
255. Arbizu J, Morbelli S, Minoshima S, Barthel H, Kuo P, Van Weehaeghe D, et al. SNMMI procedure standard/EANM practice guideline for brain [18F] FDG PET imaging, version 2.0. J Nucl Med. 2025;66:S45–60.
256. Kesner AL, Brosch-Lenz J, Gear J, Lassmann M. Dosimetry software for theranostic applications: current capabilities and future prospects. J Nucl Med. 2025;66:166–72.
257. Nadig V, Herrmann K, Mottaghy FM, Schulz V. Hybrid total-body PET scanners—current status and future perspectives. Eur J Nucl Med Mol Imaging. 2022;49:445–59.
258. Gujral K, Gujral J, Gandhi O, Singh S, Ayubcha C, Werner T, et al. An overview on current large axial field of view scanners. Soc Nuclear Med; 2025.
259. Mannheim JG, Rausch I, Conti M, la Fougère C, Schmidt FP. Characterization of the partial volume effect along the axial field-of-view of the biograph vision Quadra total-body PET/CT system for multiple isotopes. Ejnmmi Phys. 2023;10:33.
260. Panin V, Millardet M, Bharkhada D, Conti M. FastPET: Histoprojections approach. 2024 IEEE nuclear science symposium (NSS), medical imaging conference (MIC) and room temperature semiconductor detector conference (RTSD): IEEE; 2024; pp. 1–1.
261. Kaalep A, Sera T, Rijnsdorp S, Yaqub M, Talsma A, Lodge MA, et al. Feasibility of state of the art PET/CT systems performance harmonisation. Eur J Nucl Med Mol Imaging. 2018;45:1344–61.
262. Seifert R, Weber M, Kocakavuk E, Rischpler C, Kersting D, Elsevier. Artificial intelligence and machine learning in nuclear medicine: future perspectives. Semin Nucl Med. 2021. https://doi.org/10.1053/j.semnuclmed.2020.08.003.
263. Hosny A, Parmar C, Quackenbush J, Schwartz LH, Aerts HJ. Artificial intelligence in radiology. Nat Rev Cancer. 2018;18:500–10.